TURBULENCE-MODEL TRANSITION PREDICTIONS FOR BLUNT-BODY FLOWS

David C. Wilcox

DCW Industries

Prepared for:

Air Force Office of Scientific Research

July 1974

UNCLASSIFIED

SECURITY CLASSIFICATION OF THIS PAGE (When Data Entered)

AD/A-000575

REPORT DOCUMENTATION PAGE

READ INSTRUCTIONS BEFORE COMPLETING FORM

1. REPORT NUMBER: AFOSR - TR - 74 - 1714	2. GOVT ACCESSION NO.
3. RECIPIENT'S CATALOG NUMBER	
4. TITLE (and Subtitle): TURBULENCE-MODEL TRANSITION PREDICTIONS FOR BLUNT-BODY FLOWS	5. TYPE OF REPORT & PERIOD COVERED: INTERIM
6. PERFORMING ORG. REPORT NUMBER: DCW-R-03-01	
7. AUTHOR(s): DAVID C WILCOX	8. CONTRACT OR GRANT NUMBER(s): F44620-74-C-0048
9. PERFORMING ORGANIZATION NAME AND ADDRESS: DCW INDUSTRIES, 13534 VALLEY VISTA BOULEVARD, SHERMAN OAKS, CALIFORNIA 91403	10. PROGRAM ELEMENT, PROJECT, TASK AREA & WORK UNIT NUMBERS: 681307, 9781-02, 61102F
11. CONTROLLING OFFICE NAME AND ADDRESS: AIR FORCE OFFICE OF SCIENTIFIC RESEARCH/NA, 1400 WILSON BOULEVARD, ARLINGTON, VIRGINIA 22209	12. REPORT DATE: July 1974
	13. NUMBER OF PAGES: 59
14. MONITORING AGENCY NAME & ADDRESS (if different from Controlling Office)	15. SECURITY CLASS. (of this report): UNCLASSIFIED
	15a. DECLASSIFICATION/DOWNGRADING SCHEDULE

16. DISTRIBUTION STATEMENT (of this Report)

Approved for public release; distribution unlimited.

17. DISTRIBUTION STATEMENT (of the abstract entered in Block 20, if different from Report)

18. SUPPLEMENTARY NOTES

19. KEY WORDS (Continue on reverse side if necessary and identify by block number)

BOUNDARY LAYER TRANSITION
TURBULENCE PREDICTION
TRANSITION PREDICTION
BLUNT-BODY FLOWS
RE-ENTRY AEROMECHANICS

20. ABSTRACT (Continue on reverse side if necessary and identify by block number)

An accurate and efficient method has been developed for predicting transition from laminar to turbulent flow. The method is based upon a phenomenological turbulence model originally devised by Saffman for fully turbulent flows. The model is modified to account for low Reynolds number phenomena and is used to make a priori transition predictions. Primary emphasis focuses upon blunt-body flows; predict ons are also made for constant-pressure boundary-layer flows to provide as broad a data base as possible to assess model accuracy. The method yields excellent agreement between computed and experimentally measured effects

DD FORM 1 JAN 73 1473 EDITION OF 1 NOV 65 IS OBSOLETE

UNCLASSIFIED

SECURITY CLASSIFICATION OF THIS PAGE (When Data Entered)

of freedsteam turbulence, surface roughness and suction on incompressible flat-plate-boundary-layer transition. Model-predicted effects of surface roughness on transition in the vicinity of the stagnation point of a sphere-cone body virtually duplicate measured effects. The method also yields close agreement between calculated and measured surface-cooling and nose-radius effects on sphere-cone transition. Based on results obtained in the study, a blunt-body transition-prediction algorithm for use by weapon-system design engineers has been devised.

FOREWORD

This report summarizes research performed in Contract F44620-74-C-0048 during the period January 15 through July 15, 1974. The research was jointly sponsored by the Space and Missile Systems Organization and the Air Force Office of Scientific Research (AFSC), United States Air Force. The Air Force program monitors were Captain A.R. Hunt and Second Lieutenant T. Hopkins of SAMSO and Dr. M. Rogers of AFOSR. Mr. W. Portenier maintained technical liason with the Aerospace Corporation.

Participants in the study were D.C. Wilcox, principal investigator, and T.L. Chambers. Manuscript preparation was supported by B.A. Wilcox, W.A. Coonfield, and G.J. McCornock. Professor P.G. Saffman of the California Institute of Technology also made important contributions during the course of the study.

A technical note based on results obtained in this study has been submitted for publication in the AIAA Journal. The note is entitiled, "Turbulence-Model Transition Predictions" and is authored by D.C. Wilcox. Material presented in the note includes, with the exception of surface roughness effects, all significant results presented in Sections 2 and 3.

A second AIAA Journal publication is in preparation. The paper will be based on the surface-roughness analyses of Sections 3 and 4.

ABSTRACT

An accurate and efficient method has been developed for predicting transition from laminar to turbulent flow. The method is based upon a phenomenological turbulence model originally devised by Saffman for fully turbulent flows. The model is modified to account for low Reynolds number phenomena and is used to make a priori transition predictions. Primary emphasis focuses upon blunt-body flows; predictions are also made for constant-pressure boundary-layer flows to provide as broad a data base as possible to assess model accuracy. The method yields excellent agreement between computed and experimentally measured effects of freestream turbulence, surface roughness and suction on incompressible flat-plate-boundary-layer transition. Model-predicted effects of surface roughness on transition in the vicinity of the stagnation point of a sphere-cone body virtually duplicate measured effects. The method also yields close agreement between calculated and measured surface-cooling and nose-radius effects on sphere-cone transition. Based on results obtained in the study, a blunt-body transition-prediction algorithm for use by weapon-system design engineers has been devised.

CONTENTS

SECTION		PAGE
	FOREWORD	ii
	ABSTRACT	iii
	CONTENTS	iv
	NOTATION	v
1.0	INTRODUCTION	1
2.0	FORMULATION	4
	2.1 Turbulence Model Equations	4
	2.2 Low-Reynolds-Number Effects	8
	2.3 Predicted Transition Mechanism	12
3.0	CONSTANT-PRESSURE BOUNDARY-LAYER FLOWS	14
	3.1 Freestream Turbulence	14
	3.2 Surface Roughness	17
	3.3 Suction	21
	3.4 Channel and Pipe Flow	23
4.0	BLUNT-BODY FLOWS	24
	4.1 Surface Roughness	24
	4.1.1 PANT Series A Calculations	24
	4.1.2 Incipient Transition Calculations	29
	4.2 Surface Cooling	32
	4.3 Nose Radius	35
	4.4 Numerical Nosetip-Transition Correlation	41
5.0	DISCUSSION	44
	APPENDIX: THE EDDYBL COMPUTER CODE	46
	REFERENCES	49

NOTATION

SYMBOL	DEFINITION
c_f	Skin friction
C_p	Specific heat at constant pressure
C_Q	Volume coefficient
e	Specific turbulent energy
j	Index for planar (j=0) or axisymmetric (j=1) flow
k	Roughness height
M	Mach number
$N(k/\theta)$	Surface-roughness function
p, p_t	Static pressure, total pressure
Pr_L, Pr_T	Laminar and turbulent Prandtl number
$\dot{q}$, $\dot{q}_{stag}$	Local heat transfer, stagnation-point heat transfer
r	Radial body coordinate
r_N	Nose radius
Re_∞	Freestream unit Reynolds number
Re_k, Re_x, Re_θ	Reynolds number based on roughness height, plate length, momentum thickness
Re_T	Turbulent Reynolds number
$\tilde{Re}_x$	Neutral-stability Reynolds number
R_o	Empirical parameter in Saffman turbulence model
s	Arc length
$S(ku_\tau/\nu)$	Surface-roughness function
T, T_t	Static temperature, total temperature
T'	Turbulence intensity at boundary-layer edge
u	Velocity component in x direction
U_e, U_∞	Boundary-layer-edge velocity, freestream velocity
v	Velocity component in y direction
x	Coordinate lying along a solid body
y	Coordinate normal to a solid body
α, α^*	Empirical parameters in Saffman turbulence model

NOTATION (Cont.)

SYMBOL	DEFINITION
α_∞, α_∞^*	Values of α, α^* for fully turbulent flows
β, β^*	Empirical parameters in Saffman turbulence model
δ,δ^*	Boundary-layer thickness, displacement thickness
ε	Kinematic eddy viscosity
θ	Momentum thickness
κ	Karman's constant
λ	Empirical parameter in Saffman turbulence model
μ	Molecular viscosity
ν	Kinematic viscosity
ξ	Empirical parameter in Saffman turbulence model
ρ	Fluid mass density
σ, σ^*	Empirical parameters in Saffman turbulence model
ϕ	Angle from centerline for spherical body
ω	Turbulent dissipation rate
Ω	Specific turbulent dissipation rate

Subscripts

e	Boundary-layer edge
t	Transition point
w	Body surface
∞	Freestream

1.0 INTRODUCTION

An understanding of boundary-layer transition phenomena in blunt-body flows is essential to the design of reentry-vehicle nosetips. Transition sensitivity to many complicated effects must be defined; these effects include surface roughness, surface cooling, mass transfer, nosetip geometry, freestream Mach number, and freestream turbulence level. Although experimental work[1-7] has attempted to quantify the importance of these various effects, a reliable analytical tool for predicting complex-flow transition-point location remains to be developed. Since flight conditions often cannot be simulated accurately in a wind tunnel and since applicable, retrievable flight-test data are rare, accurate analytical tools are needed to facilitate extrapolation from wind-tunnel conditions to real flight conditions.

Although analytical tools for predicting transition from laminar to turbulent flow have improved significantly in recent years, transition remains one of the least-understood phenomena of fluid mechanics. Presently, analytical studies focus on the following four approaches:

1. Semiempirical Formulas

The simplest approach is to start with a physical fact or argument and devise a formula containing adjustable parameters; a classic example of this method is given by Van Driest and Blumer[8]. Such formulas can be very useful for parametric studies and for correlating experimental data for a given class of flows, but a lack of universality generally limits the utility of this approach.

2. First Principles

The most rigorous tact that can be taken is to seek

time-dependent Navier-Stokes solutions. While preliminary steps have been taken in this direction[9], required computing times are currently too lengthy to make such computations practicable for engineering applications.

3. Linear Stability Analysis

The approach which has received the greatest amount of attention is linear stability analysis[10-13]. While some insight into the transition phenomenon has attended this work, predictions often differ from experimental observations. Furthermore, linear analysis determines stability of a flow to infinitesimal disturbances only and is inapplicable when initial flow perturbations are of finite amplitude. Finally, in a linear stability analysis, complicating effects such as wall roughness, wall colling, mass transfer, and freestream turbulence level and scale considerably increase the approach's mathematical complexity.

4. Phenomenological Turbulence Models

A relatively new method offers many advantages over the approaches listed above; this method uses the Reynolds-averaged equations of motion subject to a set of closure hypotheses suitable for accurate computation through transition. This approach, on the one hand, is applicable to arbitrary amplitude disturbances and, on the other hand, in a simple and natural way can account for the complicating effects cited above. Recent progress with phenomenological-turbulence-model equations indicates this approach is sensible, i.e., that adequate closure approximations can indeed be determined. Using turbulence-model equations in which the Reynolds stresses depend upon

flow history, Donaldson[14], Jones and Launder[15], and Wilcox[16] have shown that such equations accurately predict abrupt transition from laminar to turbulent flow for constant-pressure boundary layers.

The turbulence-model approach is taken in the present study, where the primary objective has been to develop an accurate method for predicting transition in blunt-body flows, including the effects of surface roughness, surface cooling, mass transfer, blunt-body geometry, freestream Mach number, and freestream turbulence. To accomplish this objective, a series of transition-prediction computations has been performed based on the Saffman turbulence-model equations[19]. To provide a broad data base for assessing turbulence-equation accuracy, the calculations include transitional flat-plate-boundary-layer (FPBL), pipe, and channel flow in addition to the more-pertinent blunt-body-flow computations. Section 2 discusses the model equations and the method by which transition predictions are made; qualitative features of the model-predicted transition mechanism are also described. Section 3 presents transition predictions for constant-pressure boundary-layer flows and includes comparisons with experimental data. Section 4 summarizes transition predictions for blunt-body flows; based on the results presented in Section 4, a new engineering correlation is devised which can be used for predicting nosetip transition. Results of the study are summarized in Section 5.

2.0 FORMULATION

The basic analytical approach taken in the study for predicting transition is presented in this section. Subsection 2.1 presents the turbulence model equations and the method by which the equations are used to predict transition. Model revisions required for improving transition-prediction accuracy are described in Subsection 2.2. The section concludes with a discussion of the model-predicted transition mechanism.

2.1 TURBULENCE MODEL EQUATIONS

The turbulence model equations which form the basis of the present study were originally devised by Saffman[17] for incompressible flows. In subsequent development efforts[18,19], Wilcox has cast the model equations in a form suitable for compressible flow applications. The Saffman model is a two-equation model of turbulence; i.e., two nonlinear diffusion equations are solved in addition to the conservation (mass, momentum, energy) equations in computing a given flowfield. In terms of mass-averaged mean quantities[20], the coupled set of equations describing compressible boundary-layer flows over planar (j=0) or axisymmetric (j=1) surface are as follows:

Conservation of Mass

$$\frac{\partial}{\partial x}(r^j \rho u) + \frac{\partial}{\partial y}(r^j \rho v) = 0 \qquad (1)$$

Conservation of Momentum

$$\rho u \frac{\partial u}{\partial x} + \rho v \frac{\partial u}{\partial y} = -\frac{dp_e}{dx} + \frac{1}{r^j} \frac{\partial}{\partial y}\left[r^j (\mu + e/\Omega) \frac{\partial u}{\partial y}\right] \qquad (2)$$

Conservation of Energy

$$\rho u\frac{\partial}{\partial x}(C_pT) + \rho v\frac{\partial}{\partial y}(C_pT) = u\frac{dp_e}{dx} + (\mu+e/\Omega)\left(\frac{\partial u}{\partial y}\right)^2 + \frac{1}{r^J}\frac{\partial}{\partial y}\left[r^J\left(\frac{\mu}{Pr_L} + \frac{e/\Omega}{Pr_T}\right)\frac{\partial}{\partial y}(C_pT)\right] \quad (3)$$

Specific Turbulent Energy

$$\rho u\frac{\partial e}{\partial x} + \rho v\frac{\partial e}{\partial y} = [\alpha^*\left|\frac{\partial u}{\partial y}\right| - \beta^*\rho\Omega]\rho e + \xi e\left(u\frac{\partial \rho}{\partial x} + v\frac{\partial \rho}{\partial y}\right) + \frac{1}{r^J}\frac{\partial}{\partial y}\left[r^J\ (\mu+\sigma^*e/\Omega)\frac{\partial e}{\partial y}\right] \quad (4)$$

Specific Turbulent Dissipation Rate

$$\rho u\frac{\partial \Omega^2}{\partial x} + \rho v\frac{\partial \Omega^2}{\partial y} = [\alpha\left|\frac{\partial u}{\partial y}\right| - \beta\rho\Omega]\rho\Omega^2 + \frac{1}{r^J}\frac{\partial}{\partial y}\left[r^J\ (\mu+\sigma e/\Omega)\frac{\partial \Omega^2}{\partial y}\right] \quad (5)$$

In Equations (1-5), x and y are orthogonal coordinates with x lying along the body and y being normal to the surface; r is the radial body coordinate (see Figure 1). Velocity components in the x and y directions are denoted by u and v. The quantities p, ρ, and T denote pressure, density, and temperature. Molecular viscosity is the quantity μ while the eddy viscosity is given by e/Ω, the ratio of specific turbulent energy, e, to specific dissipation rate, Ω. Laminar and turbulent Prandtl numbers, Pr_L and Pr_T, appear in Equation (3) while seven empirical parameters (α, α^*, β, β^*, σ, σ^*, ξ) are contained in Equations (4 and 5). Subscript e denotes the value of a quantity at the boundary-layer edge.

With the exception of ξ, values of the empirical parameters and the turbulent Prandtl number are regarded as universal constants for fully developed turbulent flows, and their

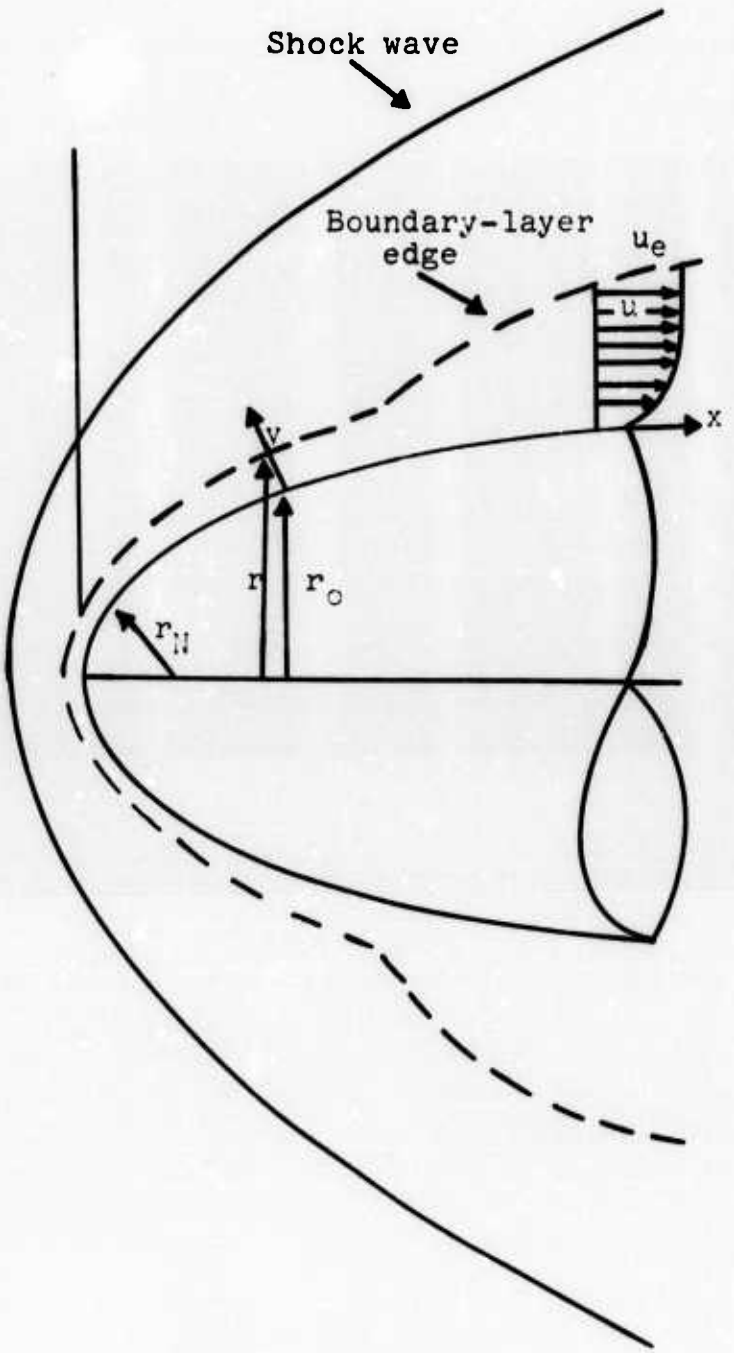

Figure 1. Coordinate system and notation.

values have been established by general arguments based on well-documented experimental observations for such flows[17-19]. The value of ξ has been selected by comparison of model predictions with experimental data for a variety of supersonic and hypersonic flows[18]. In all past calculations, values for these constants have been given by:

$$\left.\begin{aligned} Pr_T &= 0.89 \\ \xi &= 2.50 \\ \sigma^* &= 0.50 \\ \beta^* &= 0.09 \\ \alpha^* &= \alpha^*_\infty = 0.30 \\ \sigma &= 0.50 \\ 0.15 < \beta &< 0.18 \\ \alpha &= \alpha_\infty = \alpha^*_\infty[\beta/\beta^* - 4\sigma\kappa^2/\alpha^*_\infty] \end{aligned}\right\} \qquad (6)$$

where $\kappa = 0.41$ is the Karman constant.

In solving Equations (1-5), values of u, T, e and Ω are prescribed at the boundary-layer edge. The no-slip velocity boundary condition is imposed at y = 0 while either surface temperature or surface heat flux is given. Turbulent energy vanishes at y = 0 and, for perfectly smooth surfaces[19], $y^2\Omega = 20\mu/\beta\rho^2$ (the boundary condition for Ω appropriate on a rough surface is discussed in Subsection 3.2).

The Saffman turbulence model has been incorporated in a boundary-layer program developed at the NASA Langley Research Center[21]; the modified program is known as EDDYBL (see Appendix). In using EDDYBL to make boundary-layer transition predictions, specific turbulent energy and specific dissipation rate are held constant at the boundary-layer edge. Turbulent energy is set to zero throughout the boundary layer at a point near the plate leading edge. Solution of the parabolic system is accomplished by marching in the stream-

wise direction. Some entrainment and molecular diffusion of turbulent energy, e, into the boundary layer initially occurs; however little or no turbulent-energy amplification occurs for a plate-length Reynolds number below a critical value Re_{x_t}, signifying existence of laminar flow. Then, when $Re_x \geq Re_{x_t}$, an abrupt increase in e is observed, followed by an asymptote to a value characteristic of fully developed turbulent flow. The transitional regime is readily identified as the range over which e increases from its initially low level to its much higher value in the turbulent regime. The transitional regime can also be identified from the numerical data by locating abrupt changes in quantities such as momentum thickness, shape factor, and skin friction.

2.2 LOW-REYNOLDS-NUMBER-EFFECTS

In an earlier study[16], the Saffman model showed promise of being an accurate tool for transition prediction. Using the values of the empirical parameters given in Equation (6), transition was predicted for Rayleigh shear flow. Although experimental data are not available for transitional Rayleigh flow, the computed transition appeared realistic as computed Rayleigh-flow properties and measured FPBL properties were in close quantitative agreement. The first calculation in the present study was for FPBL flow so that more-direct comparison could be made between model predictions and experimental data.

Figure 2 shows computed skin friction, c_f, as a function of Re_x for an incompressible FPBL. The freestream value of e is $10^{-9}U_e^2$, where U_e is freestream velocity. As shown, the predicted transition begins at $Re_x = 4 \cdot 10^4$ and ends at $Re_x = 10^5$. The predicted value of Re_{x_t} of $4 \cdot 10^4$ is much lower than the measured Re_{x_t} for very low freestream tur-

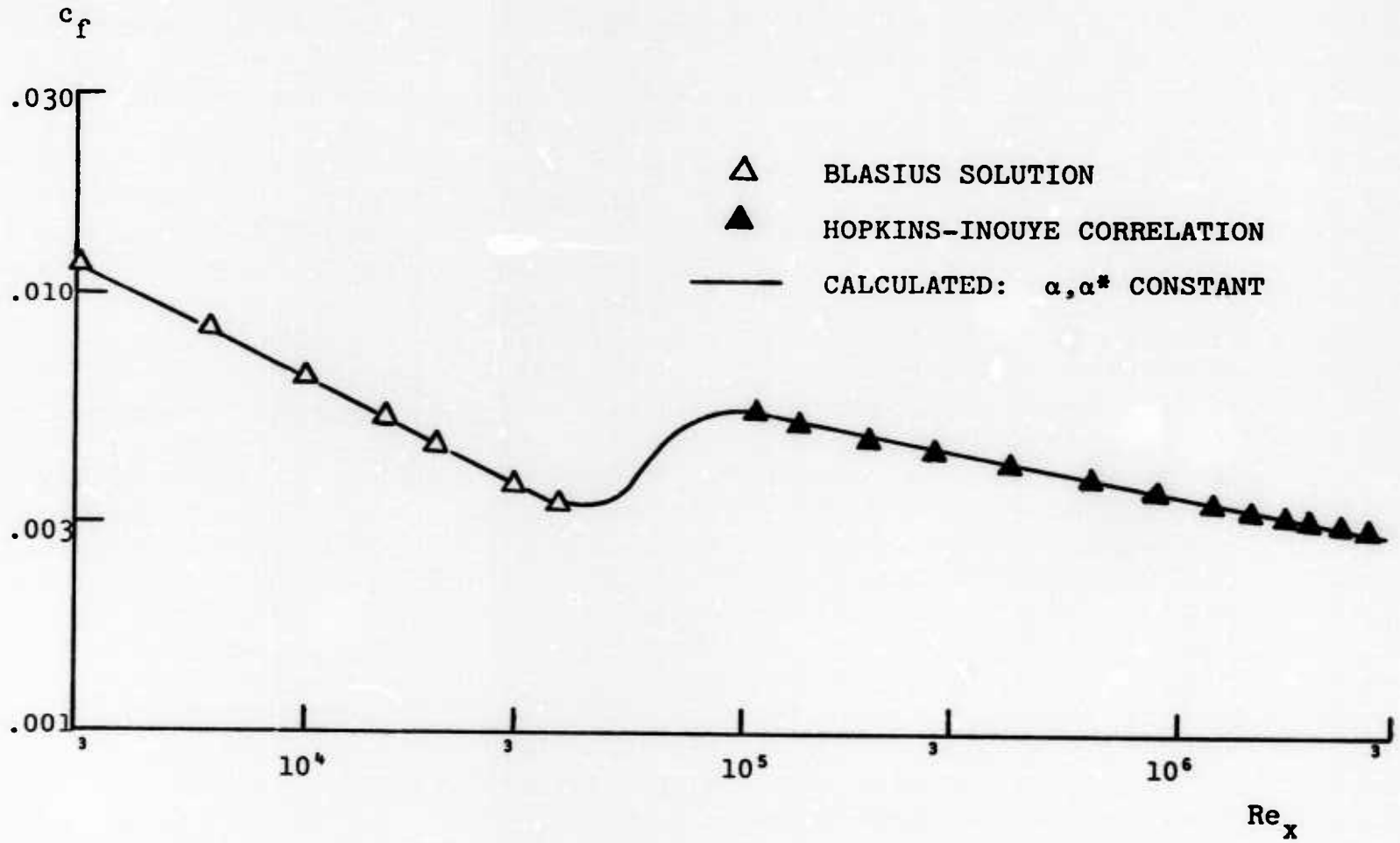

Figure 2. Skin friction as a function of plate-length Reynolds number for an incompressible FPBL.

bulence levels; Schubauer and Skramstad[5], for example, indicate that Re_{x_t} should be nearly $3 \cdot 10^6$ for $e_e \sim 10^{-7} U_e^2$.

Assuming $\alpha, \alpha^*, \beta, \beta^*, \sigma, \sigma^*, \xi$ are independent of Reynolds number leads to the inaccuracy. As noted above, the values for the empirical parameters in Equation (6) are presumed valid for fully developed turbulent flows; however, there is no a priori reason why these parameters should be independent of Reynolds number. In fact, Rotta[22] argues that such parameters depend directly upon the turbulence spectrum; since the turbulence spectrum will be quite different for low-Reynolds-number turbulence, Rotta's argument suggests that α, α^*, etc, should be Reynolds-number-dependent. Other investigators[15] have, in fact, introduced a functional dependence of similar parameters upon turbulent Reynolds number $Re_T = e/\Omega\mu$. In the present study, transition is found most sensitive to the values of α and α^*; decreasing α^* tends to delay transition while the ratio of α to α^* fixes the width of the transition zone; therefore to improve transition-prediction accuracy, an assumption is made that

$$\alpha^* = \alpha^*_\infty \left[1 - (1-\lambda)(1-Re_T/R_o)H(1-Re_T/R_o)\right] \tag{7}$$

$$\alpha/\alpha^* = \alpha_\infty/\alpha^*_\infty \tag{8}$$

where $H(x)$ is the Heaviside stepfunction and α_∞ and α^*_∞ are the values of α and α^* appropriate for fully turbulent flows [see Equation (6)].

The value of λ can be fixed by demanding that the Saffman-model neutral stability Reynolds number, $\tilde{R}e_x$, for a Blasius boundary layer be the same as that predicted by linear stability theory. Neutral stability for the turbulence model is defined as the condition where $\alpha^* |\partial u/\partial y| = \beta^* \omega$

where ω is turbulent dissipation rate[†] given by $\omega = \rho\Omega$. Then, using the Blasius velocity profile and a computed ω-profile leads to

$$\tilde{Re}_x = 1000/\lambda^2 \qquad (9)$$

with the least stable point being at approximately $y/\delta = 0.30$. Hence, using the accepted linear stability value of Re_x of $9 \cdot 10^5$, $\lambda = 0.105$. A similar argument for selecting the value of R_o remains to be found. Numerical experimentation indicates that R_o should be about 0.10, but this value should be regarded as tentative until further applications are made to determine its universality.

Finally, regarding the turbulence model and its application to transitional flows, note that algebraic transition predictions can be made which apparently are accurate to within a factor of two or three. Specifically, for many incompressible laminar flows over perfectly smooth surfaces, ω is given by $\omega = 20\nu/\beta y^2$ so that neutral stability occurs when $y^2|\partial u/\partial y|/\nu = 20/(\lambda\alpha^*_\infty\beta/\beta^*) = 317$. Also, transition will be complete when production of ω^2 exceeds ω^2 dissipation, i.e., when $y^2|\partial u/\partial y|/\nu = 20/(\lambda\alpha^*_\infty) = 722$. Therefore, an approximate transition criterion predicted by the model for incompressible flows is

$$317 < \max_y y^2|\partial u/\partial y|/\nu < 722 \qquad (10)$$

Equation (10) resembles the Van Driest-Blumer[8] formulation.

[†] When dealing with incompressible flows in this study, the turbulent dissipation rate, ω, is used in place of the specific turbulent dissipation rate, Ω.

2.3 PREDICTED TRANSITION MECHANISM

Before discussing results obtained in the present study for constant-pressure boundary-layer flows (Section 3) and blunt-body flows (Section 4), it is interesting to pause and discuss the model-predicted transition mechanism. The most-thoroughly studied flow with regard to transition is probably incompressible FPBL flow; therefore, discussion below concentrates upon the Blasius boundary layer.

As noted in Subsection 2.1, starting from the plate leading edge with $e = 0$ throughout the boundary layer and maintaining $e = e_e$ and $\omega = \omega_e$ at the boundary-layer edge ($y = \delta$), a small amount of turbulent energy is entrained beginning at the plate leading edge. This turbulent energy then spreads through the boundary layer by the action of molecular diffusion. At this point, the turbulent energy increases monatonically from zero at the plate surface to its freestream value at the boundary-layer edge.

No turbulent-energy amplification occurs for a significant distance downstream of the plate leading edge. Turbulent-energy entrainment continues and, just upstream of the neutral stability point, a spike, or local maximum, develops in the e-profile for y/δ between 0.45 and 0.60, depending upon the value of ω_e. This prediction is consistent with experimental measurements which indicates that disturbances are first amplified in a Blasius boundary layer at a point located about 60% of the way through the boundary layer. No effect on skin friction, shape factor, etc, is observed at this point. The spike diffuses toward the wall with the magnitude of the spike remaining approximately constant; then, beyond the neutral-stability point, the spike is gradually amplified. Finally, at a plate-length Reynolds number Re_{x_t}, an abrupt increase in e is

observed throughout the boundary layer, indicating the onset of transition. The spike is now located at $y/\delta = 0.2$, near the critical layer. This prediction is consistent with linear stability analysis which indicates the least-stable point in a Blasius boundary layer occurs in the critical layer. Turbulent energy is amplified to a value typical of fully turbulent flow and levels off when Re_x is two or three times Re_{x_t}. The width of the transitional region is realistic as Re_x is observed experimentally to increase typically by a similar amount through transition.

Hence, many qualitative features of FPBL transition are adequately represented in the model-predicted transition. As will be shown in the following sections, the model also yields accurate quantitative predictions for properties of engineering interest (e.g., transition Reynolds number) in both FPBL and blunt-body flows.

3.0 CONSTANT-PRESSURE BOUNDARY-LAYER FLOWS

This study's primary objective has been to develop an accurate transition-prediction method for blunt-body (e.g., RV nosetips) flows. However, a wealth of constant-pressure boundary-layer-transition data is available, including many effects pertinent to transition on reentry vehicles (RV's) under flight conditions. Hence, studying both constant-pressure boundary-layer and blunt-body flows permits a larger data base for testing model accuracy. Additionally, studying more than one class of flows may permit development of a universally applicable transition-prediction method. Calculations have thus been performed for FPBL flow, channel flow and pipe flow in addition to the more-pertinent blunt-body flows. Sensitivity of model-predicted transition for FPBL flow to freestream turbulence (Subsection 3.1), to surface roughness (Subsection 3.2), and to suction (Subsection 3.3) is determined. Channel and pipe flow are analyzed in Subsection 3.4.

3.1 FREESTREAM TURBULENCE

With α and α^* given by Equations (7 and 8), effects of freestream turbulence on incompressible FPBL transition have been analyzed. Table 1 summarizes the computations; Figure 3 compares model-predicted transition Reynolds number, Re_{x_t}, with experimental data[5,23-26]. Transition Reynolds number is defined in the computations as the point where c_f is first observed to deviate from the laminar value by more than 0.5%; turbulence intensity, T', is defined as

$$T' = 100 \sqrt{\frac{2}{3} e_e}/U_e \qquad (11)$$

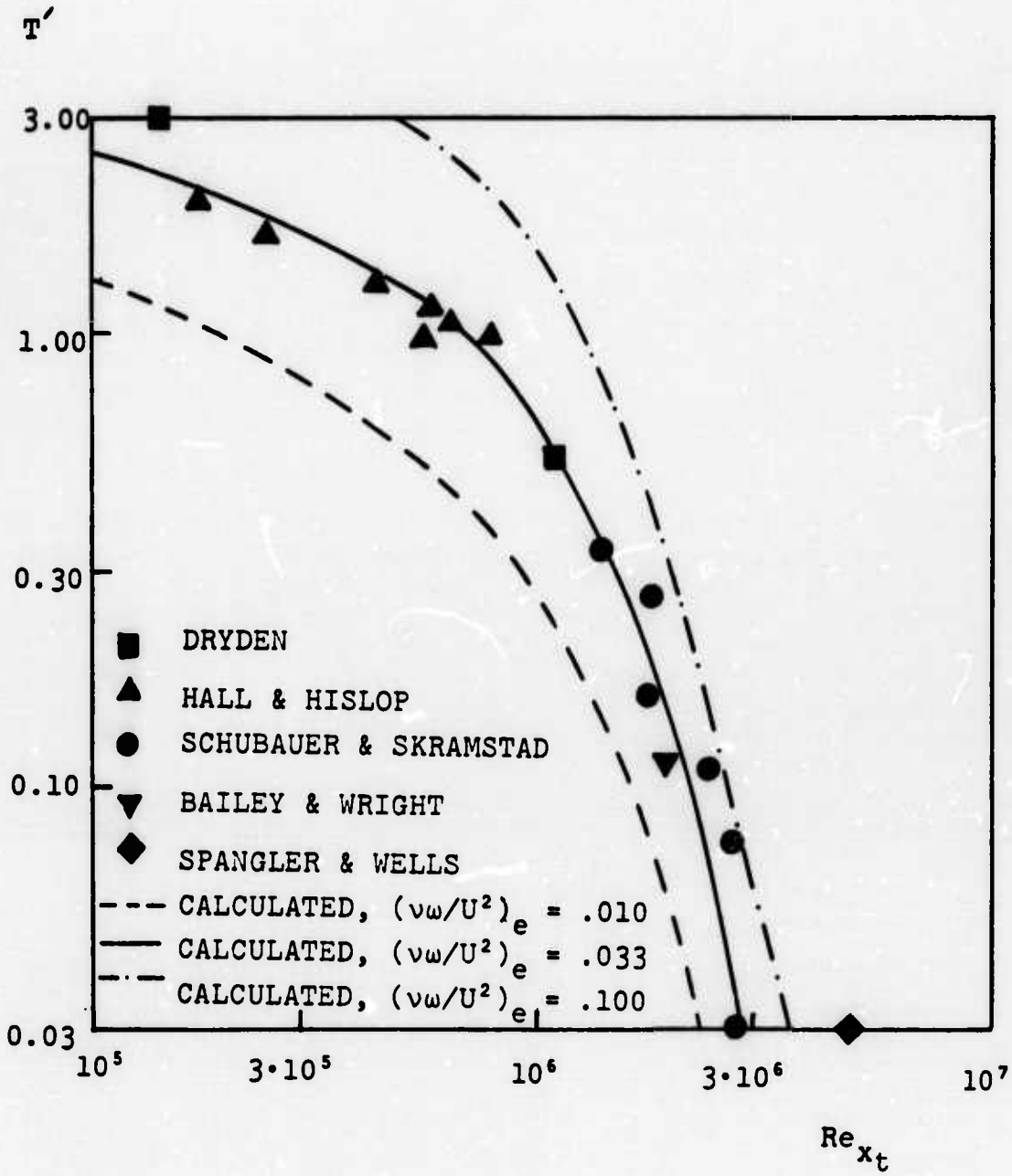

Figure 3. Transition Reynolds number for incompressible FPBL flow as a function of freestream turbulence intensity, T′.

Table 1. Freestream turbulence effects on transition Reynolds number for incompressible FPBL flow

T'	$(\nu\omega/U^2)_e$	Re_{x_t}
2.58	0.010	$1.51 \cdot 10^4$
0.60		$4.51 \cdot 10^5$
0.08		$1.73 \cdot 10^6$
0.03		$2.32 \cdot 10^6$
2.58	0.033	$9.25 \cdot 10^4$
0.60		$1.02 \cdot 10^6$
0.08		$2.27 \cdot 10^6$
0.03		$2.86 \cdot 10^6$
2.58	0.100	$5.95 \cdot 10^5$
0.60		$1.58 \cdot 10^6$
0.08		$2.77 \cdot 10^6$
0.03		$3.37 \cdot 10^6$

As shown in Figure 3, model-predicted transition occurs at much higher values of Re_x than were obtained when α^* was assumed independent of Re_T.

An important feature of the model is that it characterizes freestream turbulence (as would be expected on physical grounds) with two quantities, viz, intensity and scale. In addition to freestream turbulent energy, the turbulent dissipation rate ω, must be specified; this boundary condition is equivalent to specification of a turbulence scale. The effect of the freestream value of ω on predicted transition is also shown in Figure 3. The effect of ω_e is most pro-

nounced for high-intensity turbulence, with increasing ω_e tending to delay transition. Excellent agreement with all data shown is obtained when $\nu\omega_e/U_e = .033$.

3.2 SURFACE ROUGHNESS

Surface roughness has been represented with the turbulence model[17] for fully developed turbulent flows by using the following dissipation rate boundary condition:

$$\omega = \frac{S}{\alpha_\infty^*} \frac{u_\tau^2}{\nu} \qquad \text{at } y = 0 \tag{12}$$

where u_τ is friction velocity and S is a function of surface roughness. Saffman and Wilcox[19] have correlated S with roughness height, k, and arrived at the relation

$$ku_\tau/\nu = 50\ S^{-1/2} \tag{13}$$

Combining Equations (12 and 13) there follows

$$\omega = \frac{2500}{\alpha_\infty^*} \frac{\nu}{k^2} \qquad \text{at } y = 0 \tag{14}$$

Equation (14) has been developed with the hypothesis that the roughness element is very small compared to a typical boundary layer dimension such as momentum thickness, θ. This hypothesis is valid for roughness heights of practical interest (i.e., roughness-height Reynolds number, Re_k, up to 1000) when a boundary layer is turbulent. However, for laminar boundary layers, even relatively small roughness heights will be comparable to the boundary-layer thickness. For example, when $Re_k > 150$, a roughness element is more than 10% of the boundary-layer thickness when $Re_x = 10^5$, a clear violation of the original postulates made in arriving at Equation (14).

A more general boundary condition has been devised in the present study, namely,

$$\omega = \frac{2500}{\alpha_\infty^*} N(k/\theta) \frac{\nu}{k^2} \tag{15}$$

where

$$N(k/\theta) \to 1 \text{ as } k/\theta \to 0 \tag{16}$$

To help deduce the functional dependence of N upon k/θ, a simple correlation between Re_k and the value of ω at a solid boundary has been inferred from experimental data of Feindt[7] for incompressible rough-wall FPBL flow. The correlation was developed by numerical experimentation which showed that the Feindt data are duplicated by model-equation predictions using the generalized boundary condition (15) with the quantity N given by

$$N = \frac{16}{9} [120/Re_k]^6 \tag{17}$$

Figure 4 shows the model predicted effect of surface roughness on FPBL transition when Equation (17) is used. Calculations were performed with $T' = 1\%$ and $(\nu\omega/U)_e = .033$; results of the calculations are listed in Table 2.

While excellent agreement with experimental data has been obtained using Equation (17), the formulation is not quite complete; that is, the form of the experimental data makes it convenient to infer N directly as a function of Re_k. While Re_k is certainly of importance in rough-wall transition, k/θ is a more fundamental parameter since it provides a criterion for specifying when a roughness element is large compared to boundary-layer thickness while the roughness-height Reynolds number Re_k does not. How-

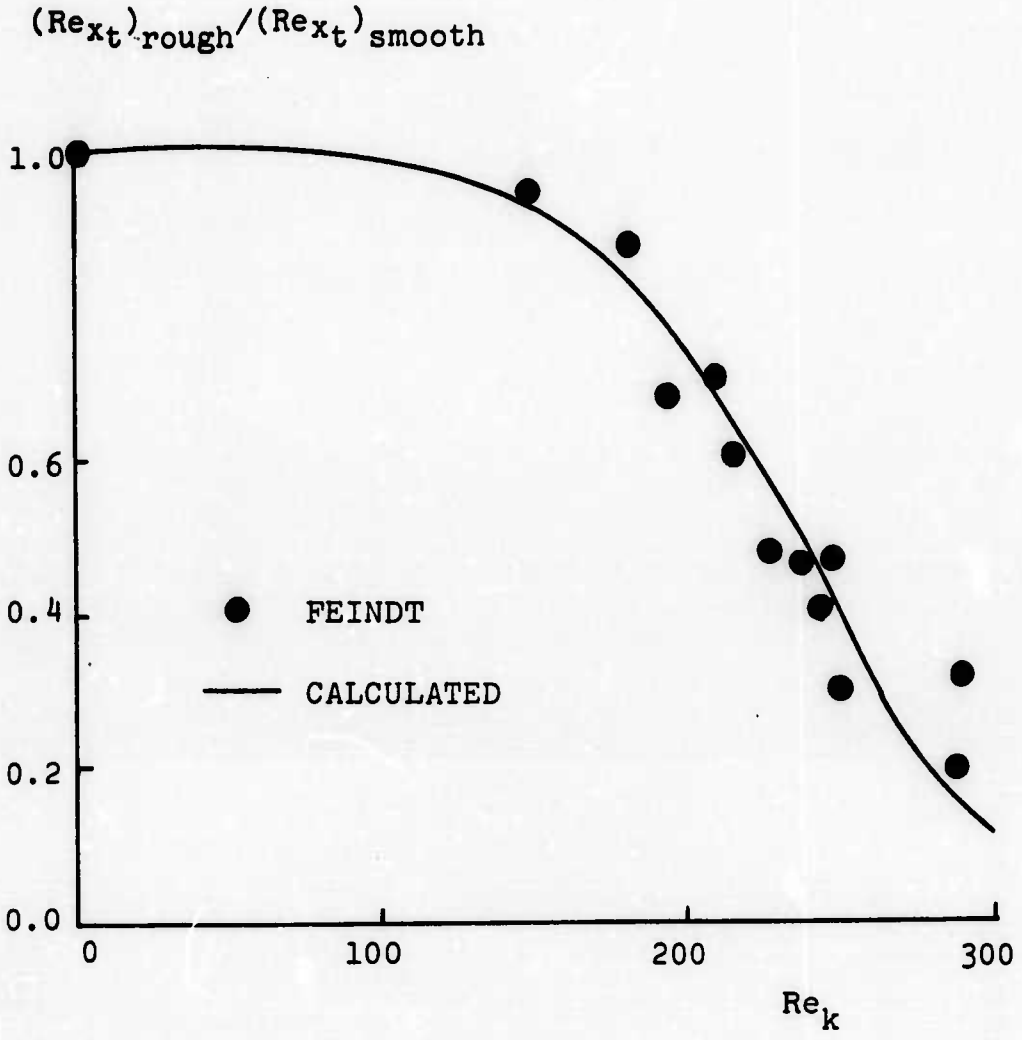

Figure 4. Transition Reynolds number for flat-plate-boundary-layer flow as a function of Reynolds number based on roughness height, Re_k.

ever, a dependence of N upon k/θ is implicitly contained in Equation (17) and can be made explicit by noting that for laminar FPBL flow

$$c_f Re = (.664)^2 \tag{18}$$

wherefore N can be rewritten as

$$N(k/\theta) = \begin{cases} 1 & , \quad \frac{k}{\theta} < 300c_f \\ \left[\frac{300c_f}{k/\theta}\right]^6 & , \quad \frac{k}{\theta} < 300c_f \end{cases} \tag{19}$$

Equations (15 and 19) are regarded as the revised rough-wall boundary condition valid for both high- and low-Reynolds-number boundary layers. For the compressible flow applications of Section 4, c_f is defined in terms of surface density, ρ_w, so that

$$c_f = 2\tau_w/\rho_w U_e^2 = (u_\tau/U_e)^2 \tag{20}$$

where τ_w is surface shear stress.

Table 2. Surface roughness effects on transition Reynolds number for incompressible FPBL flow

Re_k	$(Re_{x_t})_r$	$(Re_{x_t})_r/(Re_{x_t})_s$
0	$6.70 \cdot 10^5$	1.00
108	$6.55 \cdot 10^5$	0.98
162	$5.95 \cdot 10^5$	0.89
193	$5.19 \cdot 10^5$	0.77
219	$4.13 \cdot 10^5$	0.62
229	$3.61 \cdot 10^5$	0.54
261	$1.98 \cdot 10^5$	0.30
300	$8.25 \cdot 10^4$	0.12

3.3 SUCTION

Applications in the preceding two subsections have served mainly to fix the value of the empirical constant R_o [Equation (7)] and to determine the analytical dependence of the function N upon k/θ [Equations (15, 19, and 20]. To test the modified turbulence model with no further parameter adjustment, the effects of suction on FPBL transition have been analyzed. Computations have been performed for several suction rates (Table 3) to determine the minimum amount of suction required to prevent transition; for all calculations T' = 2.6% and $(\mu\Omega/U)_e = .033$.

Table 3. Effects of suction on transition Reynolds number for incompressible FPBL flow

C_Q	Re_{x_t}	C_Q	Re_{x_t}
0	$9.25 \cdot 10^4$	$1.5 \cdot 10^{-3}$	$3.92 \cdot 10^5$
$1.0 \cdot 10^{-4}$	$1.05 \cdot 10^5$	$1.6 \cdot 10^{-3}$	$6.03 \cdot 10^5$
$1.0 \cdot 10^{-3}$	$1.86 \cdot 10^5$	$1.7 \cdot 10^{-3}$	$> 6.59 \cdot 10^6$
$1.4 \cdot 10^{-3}$	$3.14 \cdot 10^5$	$1.8 \cdot 10^{-3}$	$> 6.59 \cdot 10^6$

Results of the calculations are shown in Figure 5; C_Q is volume coefficient defined as

$$C_Q = -v_w/U_e \tag{21}$$

where v_w is the suction velocity. The indicated minimum volume coefficient required to prevent transition is

$$C_{Qmin} \doteq .0017 \tag{22}$$

No transition occured in calculations having $C_Q > C_{Qmin}$.

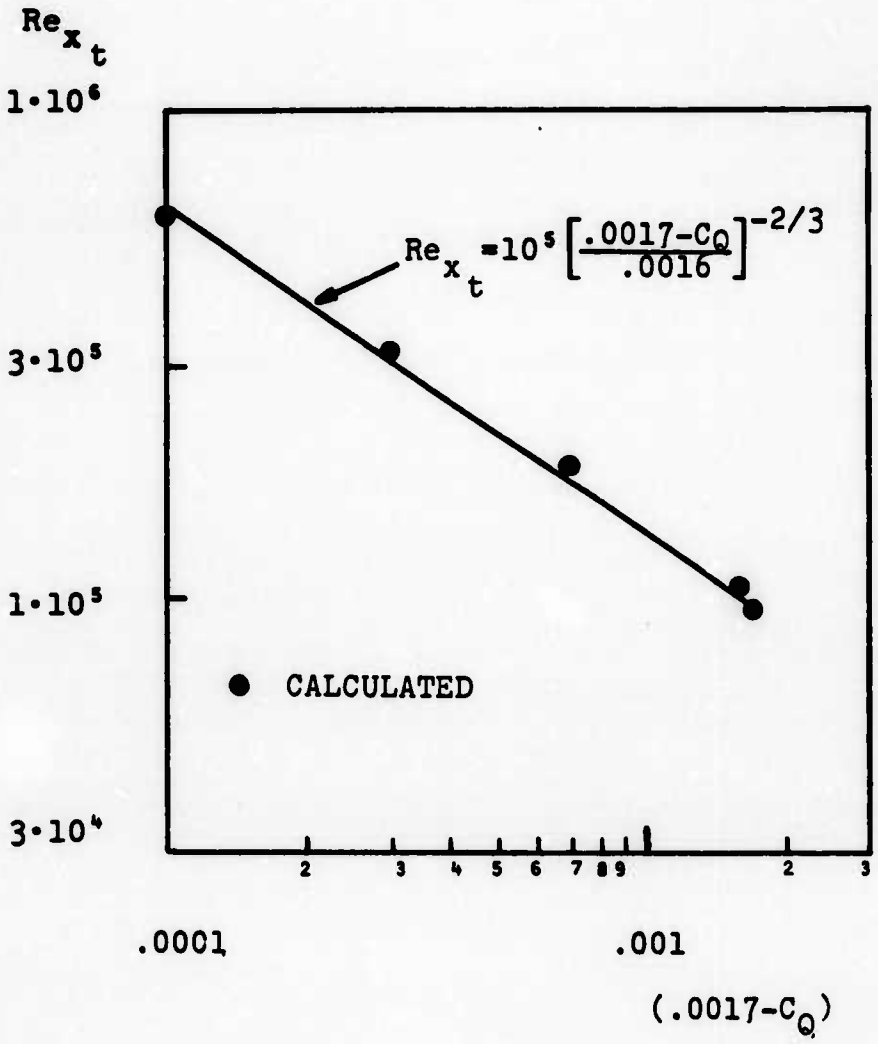

Figure 5. Transition Reynolds number for incompressible flat-plate-boundary-layer flow with uniform suction as a function of volume coefficient, C_Q.

Experimental data are sparse and inconclusive for transitional FPBL flow with suction. Experiments by Simpson, Kays and Moffat[27] for uniform suction indicate that C_{Qmin} lies between .0024 and .0046, while Pfenninger's[28] experiments suggest that C_{Qmin} is within the range .0010 to .0020. The computed C_{Qmin} is hence within experimental data scatter. As a final note, the calculated results are far more accurate than the linear stability prediction[29] of $C_{Qmin} = 1.18 \cdot 10^{-4}$.

3.4 CHANNEL AND PIPE FLOW

Fully developed channel and pipe flow are especially simple to analyze using the approximate transition criterion given in Equation (10). Table 4 summarizes predictions for transition Reynolds number, $\bar{R}$, based on average velocity and channel height/pipe diameter; experimentally measured $\bar{R}$ and the value of $\bar{R}$ predicted by linear stability analysis are also included in the table. Computed $\bar{R}$ agrees closely with measured $\bar{R}$ for both flows. As with the analysis of suction, model predictions are much closer to corresponding measurements than are linear stability predictions, particularly for pipe flow.

Table 4. Transition Reynolds number predictions for fully developed channel and pipe flow.

Flow	$\bar{R}$, Present Analysis	$\bar{R}$, Measured	$\bar{R}$, Linear Stability Analysis
Channel	1427-3249	1400	7085
Pipe	1070-2437	2300	∞

4.0 BLUNT-BODY FLOWS

Results presented in the preceding section for incompressible constant-pressure boundary-layer flows serve mainly to improve the turbulence model's transition predictive accuracy. In this section, the model is applied, with no further modification, to blunt-body flows. In Subsections 4.1 throgh 4.3, effects of surface roughness, surface cooling, and body geometry are analyzed for sphere-cone bodies immersed in a supersonic stream. Subsection 4.4 presents a transition-prediction correlation based on the numerical results.

4.1 SURFACE ROUGHNESS

Two rounds of surface-roughness calculations were performed. First, as a preliminary test of the model's accuracy for blunt-body flows, four cases from the PANT Series A Wind Tunnel Tests[2] were simulated. The body considered in the PANT Series A tests for the cases selected was a sphere-cone configuration with a nose radius, r_N, of 2.5 in. Then, for the same body at flow conditions close to those in the PANT Series A experiments, conditions for incipient transition were determined.

4.1.1 PANT Series A Computations

The cases considered, including flow conditions, are summarized in Table 5. As indicated in the table, roughness height, k, varies from 1.5 mils to 10 mils. For all cases the surface temperature, T_w, is assumed to be

$$T_w/T_{t_\infty} = 0.4 \tag{23}$$

where T_{t_∞} is the freestream total temperature. The modified Newtonian pressure distribution is used to define

boundary-layer-edge pressure, i.e.,

$$p_e/\rho_\infty U_\infty^2 = (p_{t_2}/\rho_\infty U_\infty^2 - 1) + \cos^2 \phi \qquad (24)$$

where p_{t_2} is total pressure behind the shock, ϕ is angle from the centerline, ρ_∞ is freestream density, and U_∞ is freestream velocity. In all calculations, freestream turbulence intensity is T' = 0.33% while the freestream specific dissipation rate, Ω_e, is given by

$$\Omega_e = 0.0033\ U_e^2/\mu_e \qquad (25)$$

This value for Ω_e is somewhat lower than the values used in the FPBL calculations of Section 3. This lower value is used because larger values of Ω_e cause, for reasons unknown, convergence problems near the stagnation point.

Table 5. Flow conditions for blunt-body roughness calculations.

PANT Run No.	k(mils)	M_∞	$Re_\infty(ft^{-1})$	$p_{t\infty}$(psia)	T_{t_∞}(°F)
115	1.5	4.98	$4.10 \cdot 10^6$	240	750
129	3.0	4.97	$2.05 \cdot 10^6$	123	770
164	10.0	4.98	$0.55 \cdot 10^6$	31	735
165	10.0	4.96	$0.84 \cdot 10^6$	49	742

Transition location is identified by inspecting computed surface heat transfer distribution, $\dot{q}$. For example, Figure 6 shows the computed variation of $\dot{q}$ for PANT Series A Run 165 as a function of arc length, s. The ratio of $\dot{q}$ to its value at the stagnation point, $\dot{q}_{stag}$, falls off gradually as s/r_N increases. An abrupt increase in heat transfer occurs near $s/r_N = 0.38$; $\dot{q}/\dot{q}_{stag}$ achieves a maximum value of 2.36 at

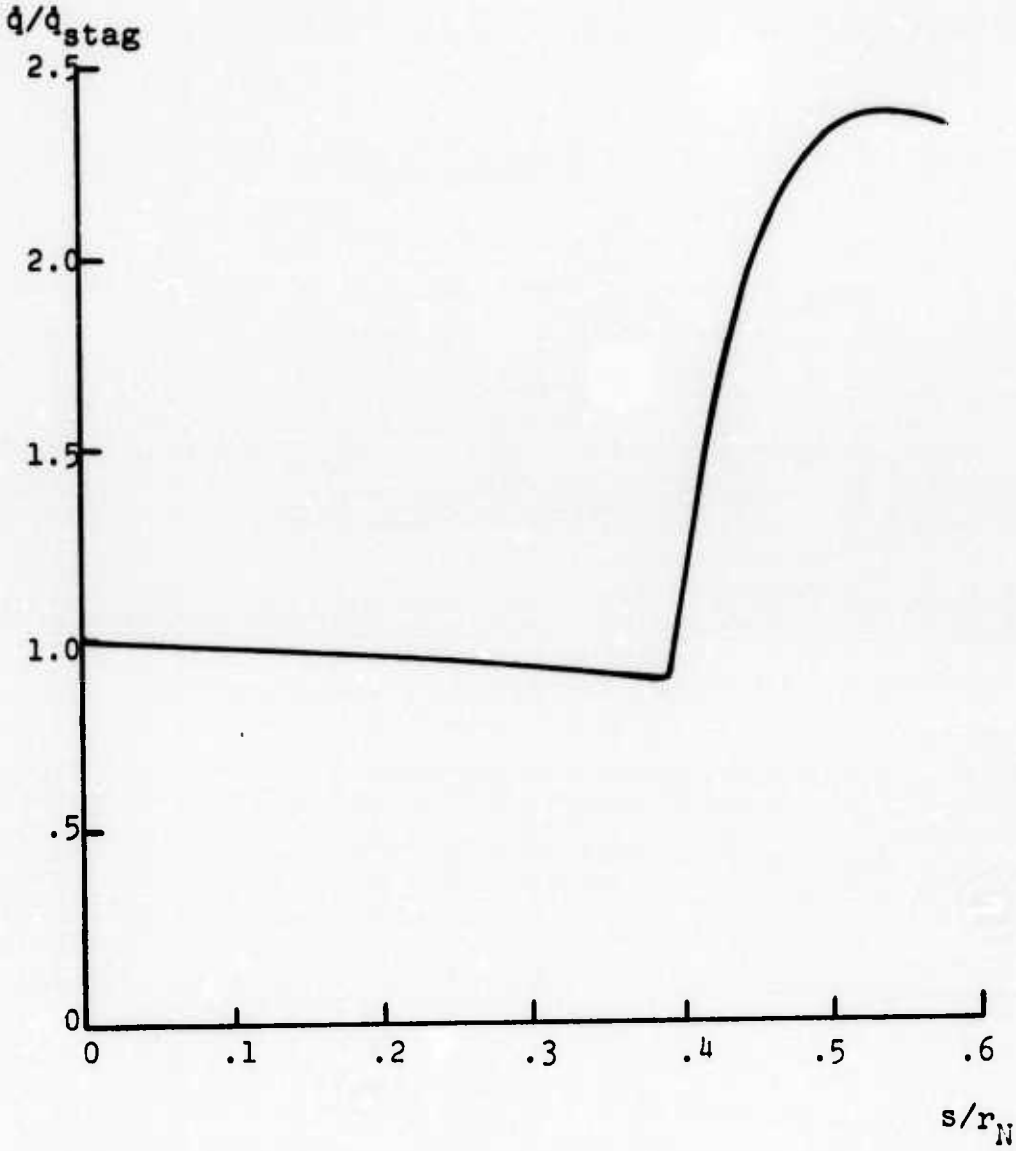

Figure 6. Heat transfer as a function of arc length for flow near the stagnation point of a sphere-cone body; PANT Series A Run 165.

$s/r_N = 0.54$, and then gradually decreases. For engineering purposes, the point at which $\dot{q}$ first increases marks the beginning of transition; similarly, the end of transition could be defined as the point where $\dot{q}$ passes its maximum value.

Table 6 summarizes results of the calculations. Transition is predicted in three of the four cases. For the three transitional cases, Figure 7 shows computed transition Reynolds number based on momentum thickness, Re_{θ_t}, as a function of $(k/\theta_t)/(T_w/T_e)$. The figure shows clearly that computed values of Re_{θ_t} for these three cases closely approximate the PANT correlation[1,2], namely,

$$Re_{\theta_t} = 215 \left[\frac{k}{\theta_t} / \frac{T_w}{T_e} \right]^{-0.7} \qquad (26)$$

For the one laminar run, PANT Run 164, no transition was predicted although computation was carried out to $\phi = 45°$, a point well beyond the sonic point. Again, the results agree with measurements, as PANT Run 164 remains laminar.

Table 6. Computed transition Reynolds numbers for blunt-body roughness calculations

PANT Run No.	k/θ_t	$\frac{k}{\theta_t} / \frac{T_w}{T_e}$	Re_{θ_t}
115	1.48	3.51	101.7
129	2.07	4.84	80.5
164	-	-	∞
165	4.50	10.74	44.0

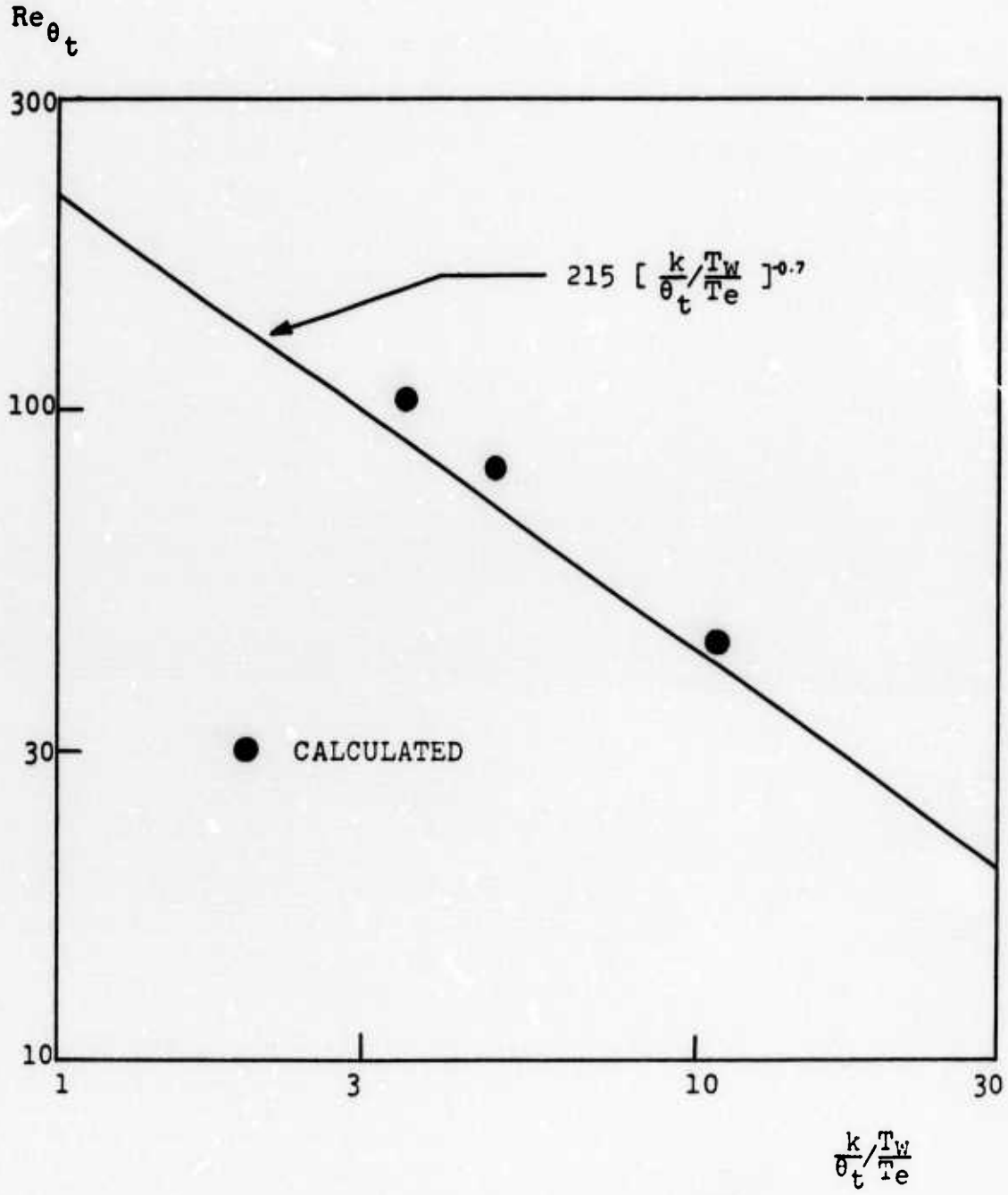

Figure 7. Transition Reynolds number based on momentum thickness as a function of roughness height for flow near the stagnation point of a sphere-cone body.

4.1.2 Incipient Transition Calculations

Knowledge of incipient transition conditions is important in reentry vehicle nosetip design. Hence, to provide a further test of the model's ability to predict salient features of blunt-body transition, a series of calculations was performed to determine, as a function of roughness height, k, the minimum freestream unit Reynolds number, Re_∞, at which transition occurs, i.e., the incipient-transition Re_∞. Again, computations were for flow near the stagnation point of a sphere-cone body having a nose radius, r_N, of 2.5 inches. For simplicity, in all calculations freestream Mach number, M_∞, and freestream total temperature, T_{t_∞}, were 5 and 750°F., respectively; surface temperature was $0.4T_{t_\infty}$. The values of T' and $(\mu\Omega/U^2)_e$ were 0.33% and 0.0033.

Four roughness heights were considered, namely, 0.5 mil, 1.5 mils, 3 mils and 10 mils. Table 7 summarizes results, including momentum thickness at the stagnation point, θ_{stag}; transition point values of angle, ϕ_t, boundary-layer-edge Mach number, M_{e_t}, displacement thickness, δ_t^*, and momentum thickness, θ_t; and the PANT coordinates, $(k/\theta_t)/(T_w/T_e)$ and Re_{θ_t}.

Figure 8 illustrates calculated behavior for k = 3 mils. Each symbol denotes transition-point location. As shown, four of the points lie along the numerical transition correlation (NTC) line defined by

$$Re_{\theta_t} = 245 \left[\frac{k}{\theta_t} \Big/ \frac{T_w}{T_e} \right]^{-0.7} \qquad (27)$$

which is very close to the PANT correlation [Equation (26)].

Table 7. Summary of incipient-transition surface-roughness calculations.

k(mils)	$Re_\infty(ft^{-1})$	θ_{stag}(mils)	ϕ^t(°)	M_e^t	δ_t^*(mils)	θ_t(mils)	$\frac{k}{\theta_t} / \frac{T_w}{T_e}$	Re_{θ_t}
0.5	$8.42 \cdot 10^6$	0.66	21.5	0.48	0.39	0.70	1.71	134
	$6.00 \cdot 10^6$	0.78	27.2	0.61	0.52	0.86	1.35	142
	$4.00 \cdot 10^6$	0.96	40.2	0.96	0.84	1.20	0.88	164
	$3.70 \cdot 10^6$	1.00	46.2	1.15	1.05	1.36	0.73	177
	$3.60 \cdot 10^6$	1.01	49.8	1.27	1.20	1.46	0.65	186
	$3.55 \cdot 10^6$	1.02	52.8	1.39	1.35	1.57	0.57	193
	$3.50 \cdot 10^6$	1.02	-	-	-	-	-	∞
1.5	$4.00 \cdot 10^6$	0.96	23.9	0.53	0.60	1.03	3.45	103
	$3.00 \cdot 10^6$	1.11	36.3	0.85	0.88	1.32	2.48	130
	$2.70 \cdot 10^6$	1.17	51.7	1.34	1.49	1.76	1.56	166
	$2.65 \cdot 10^6$	1.18	-	-	-	-	-	∞
3.0	$2.00 \cdot 10^6$	1.36	27.8	0.63	0.91	1.50	4.64	83
	$1.75 \cdot 10^6$	1.45	35.2	0.82	1.13	1.70	3.88	97
	$1.65 \cdot 10^6$	1.49	42.6	1.03	1.42	1.92	3.22	111
	$1.63 \cdot 10^6$	1.50	47.3	1.18	1.64	2.09	2.81	120
	$1.62 \cdot 10^6$	1.50	56.4	1.54	2.34	2.56	1.99	137
	$1.60 \cdot 10^6$	1.51	-	-	-	-	-	∞
10.0	$0.80 \cdot 10^6$	2.15	23.4	0.52	1.34	2.29	10.34	45
	$0.70 \cdot 10^6$	2.28	27.8	0.63	1.55	2.53	9.15	49
	$0.60 \cdot 10^6$	2.46	36.0	0.84	1.98	2.94	7.45	58
	$0.58 \cdot 10^6$	2.52	39.6	0.94	2.20	3.12	6.49	62
	$0.55 \cdot 10^6$	2.59	-	-	-	-	-	∞

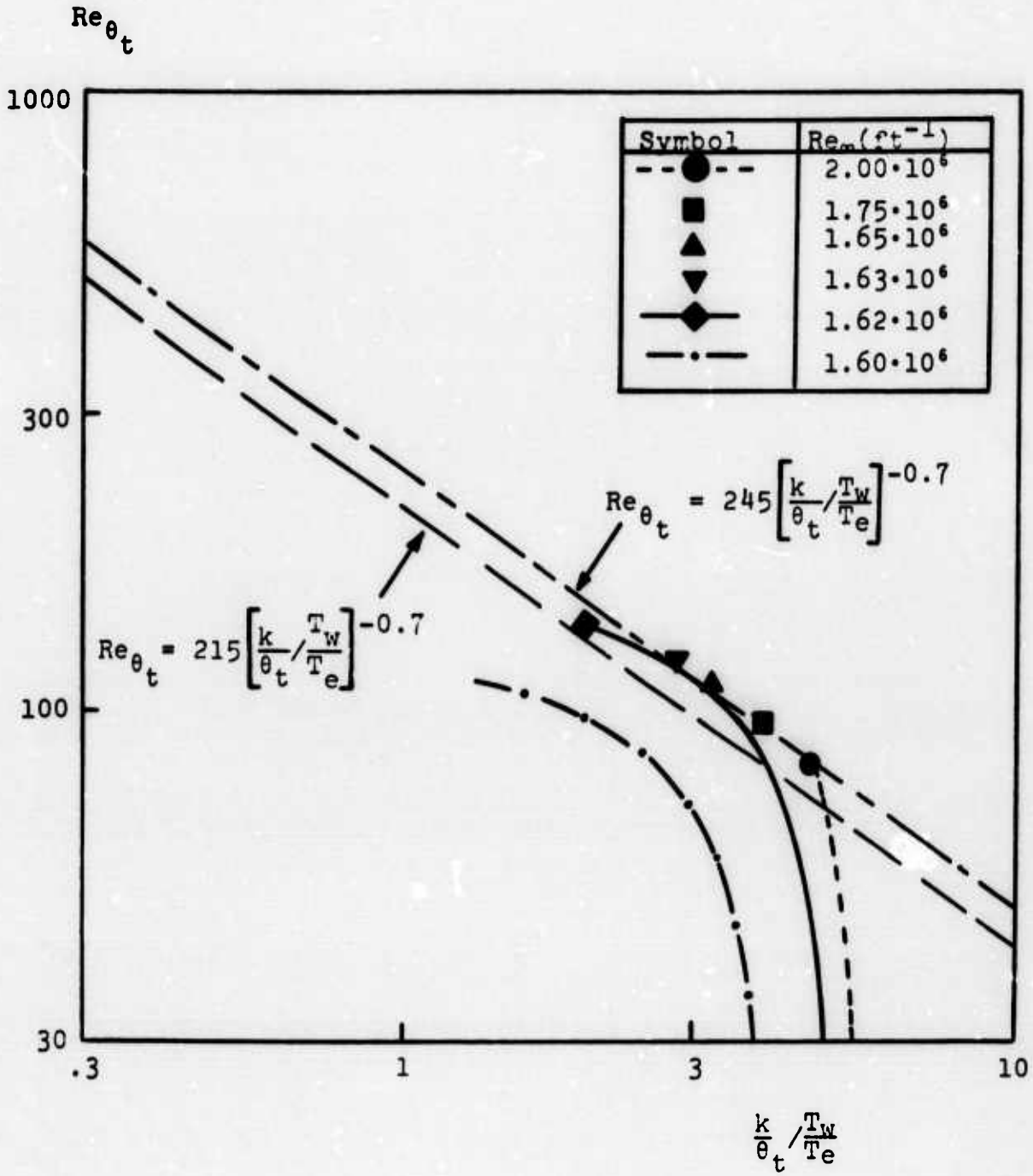

Figure 8. Illustration of the method for locating incipient-transition freestream unit Reynolds number; k = 3 mils; T_w/T_{t_∞} = 0.4.

The point for $Re_\infty = 1.62 \cdot 10^6 ft^{-1}$ is the incipient case and lies slightly below the NTC line. The three curves (referred to as Re_θ trajectories) are based on computed values of Re_θ and $(k/\theta)/(T_w/T_e)$ up to transition. On the one hand, for $Re_\infty = 2 \cdot 10^6 ft^{-1}$ the Re_∞ trajectory intersects the NTC line, and transition occurs at the intersection; on the other hand, when $Re_\infty = 1.60 \cdot 10^6 ft^{-1}$, the Re_θ trajectory never intersects the line and no transition occurs. The incipient case lies between these two extremes. As shown in Figure 8, the Re_θ trajectory is tangent to the NTC line. However, transition does not occur at the point which would be about midway between the NTC line and the PANT correlation curve. This behavior is consistent with claims that transition location and transition onset (i.e., incipient transition location) are not coincident.

Figure 9 shows that, with the exception of the 0.5-mil case, all the computed transition-point locations listed in Table 7 lie along the NTC line. Since corresponding experimental data also defy correlation, the fact that 0.5-mil numerical data fail to correlate lends further confidence to the predictions. As with the 3-mil case, the incipient transition point lies below the NTC line when k = 1.5 mils and k = 10 mils. Figure 10 presents computed incipient-transition Re_∞ as a function of k; computed values are very close to measured values[2].

4.2 SURFACE COOLING

As with surface roughness, effects of surface cooling on transition for the $r_N = 2.5$-in., sphere-cone body have been analyzed in two steps. In the first step, k and Re_∞ remain constant, and T_w/T_{t_∞} is varied. In the second step,

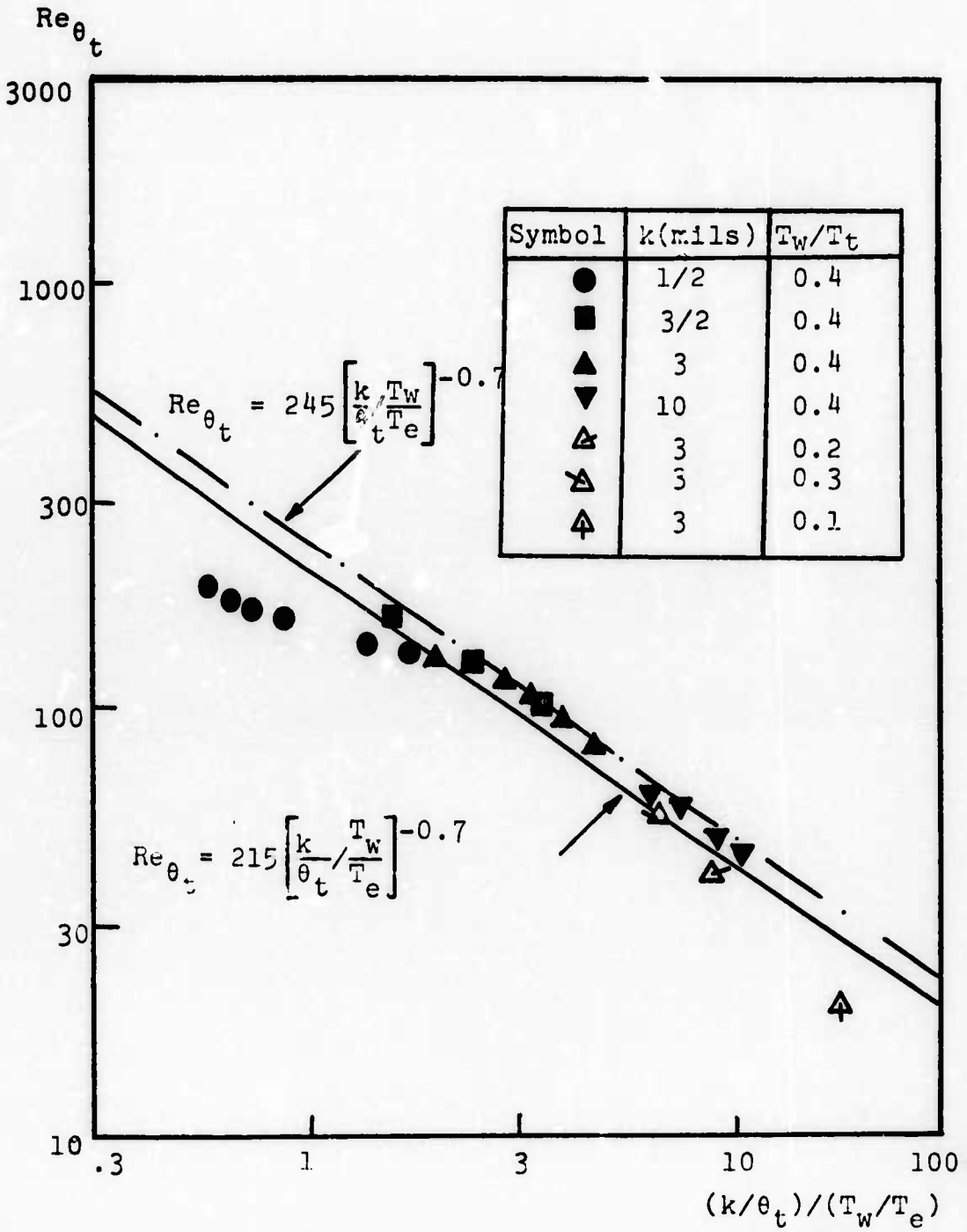

Figure 9. Summary of surface roughness and surface temperature calculations for sphere-cone stagnation-region flow.

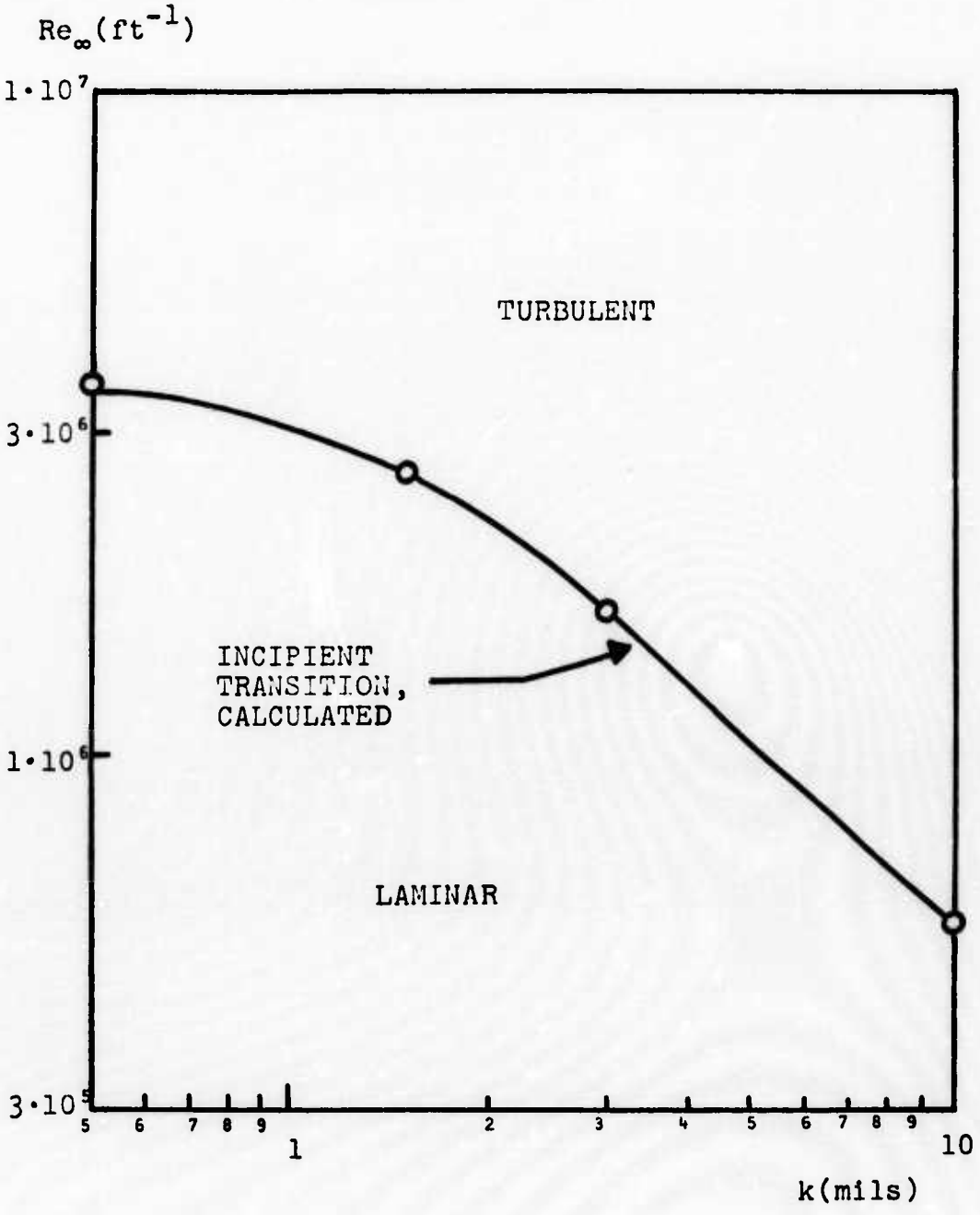

Figure 10. Freestream unit Reynolds number for incipient transition as a function of roughness height; $T_w/T_{t_\infty} = 0.4$.

with Re_∞ held constant, k is varied for $T_w/T_{t_\infty} = 0.2$ and 0.8 until incipient transition conditions are determined.

For the first set of calculations, the roughness height is 3 mils and the corresponding incipient-transition Re_∞ for $T_w/T_{t_\infty} = 0.4$ of $1.62 \cdot 10^6$ is used. As summarized in Table 8, surface temperature is varied from 0.1 to 0.8; computed Re_{θ_t} is shown graphically in Figure 11 as a function of T_w/T_{t_∞}. As would be consistent with experimental measurements for sphere-cones, surface cooling is predicted to have a destabilizing effect on transition. Figure 9 shows that for $T_w/T_{t_\infty} \geq 0.2$, predicted transition location is close to the PANT correlation line. However, for $T_w/T_{t_\infty} = 0.1$, Re_{θ_t} is about 40% lower than the PANT-correlation value.

In the second set of surface-cooling calculations, Re_∞ is $1.62 \cdot 10^6$; k is then varied for $T_w/T_{t_\infty} = 0.2$ and 0.8 until incipient-transition conditions have been determined. Results of the calculations are summarized in Table 8 and Figure 12. An approximate fit to the numerical data for the incipient-transition roughness height, k_{incip}, is

$$k_{incip} = 10 \, (T_w/T_{t_\infty})^{7/5} \qquad (28)$$

with k_{incip} given in mils.

4.3 BODY GEOMETRY

Effects of body geometry were analyzed by computing incipient-transition conditions for sphere-cones of varying nose radius. For all of the calculations, the following conditions have been used:

$$\left.\begin{array}{ll} M_\infty = 5 & T_{t_\infty} = 1340^\circ \text{ R.} \\ T_w = 500^\circ \text{ R.} & k = 3.5 \text{ mils} \\ T' = 0.33\% & \Omega_e = 0.0033 \, U_e/\mu_e \end{array}\right\} \qquad (29)$$

Table 8. Summary of surface-cooling calculations.

T_w/T_{t_∞}	k(mils)	θ_{stag}(mils)	ϕ^t(°)	M_e^t	δ_t^*(mils)	θ_t(mils)	$\frac{k}{\theta_t}/\frac{T_w}{T_e}$	Re_{θ_t}
0.10	3.00	1.67	6.6	0.14	0.42	1.68	17.78	21
0.20		1.62	13.8	0.30	0.03	1.67	8.90	41
0.30		1.56	23.4	0.52	0.51	1.66	5.69	66
0.38		1.51	36.6	0.86	1.11	1.81	3.80	97
0.45		1.48	-	-	-	-	-	∞
0.80		1.30	-	-	-	-	-	∞
0.20	2.00	1.62	20.4	0.45	0.06	1.70	5.65	60
	1.50		28.1	0.63	0.10	1.80	3.86	82
	1.00		50.3	1.29	0.45	2.44	1.54	138
	0.98		53.6	1.42	0.55	2.63	1.33	146
	0.97		56.1	1.53	0.65	2.81	1.18	152
	0.95		-	-	-	-	-	∞
0.80	10.00	1.30	27.0	0.61	2.55	1.40	8.29	62
	8.00		36.9	0.86	2.99	1.51	5.76	82
	7.50		52.3	1.37	4.49	1.86	3.67	105
	7.49		-	-	-	-	-	∞

Boundary-layer-edge pressure is again given by the modified Newtonian distribution [Equation (24)]. Three nose radii are considered, namely, 0.75 in., 2.5 in. and 3.5 in.; Table 9 summarizes the calculations. As shown in Figure 13, r_N has only a slight effect on the incipient-transition Re_∞, with increasing nose radius yielding lower values for Re_∞. This trend is consistent with recent measurements[31], thus providing another test of the theory. The numerical data are closely

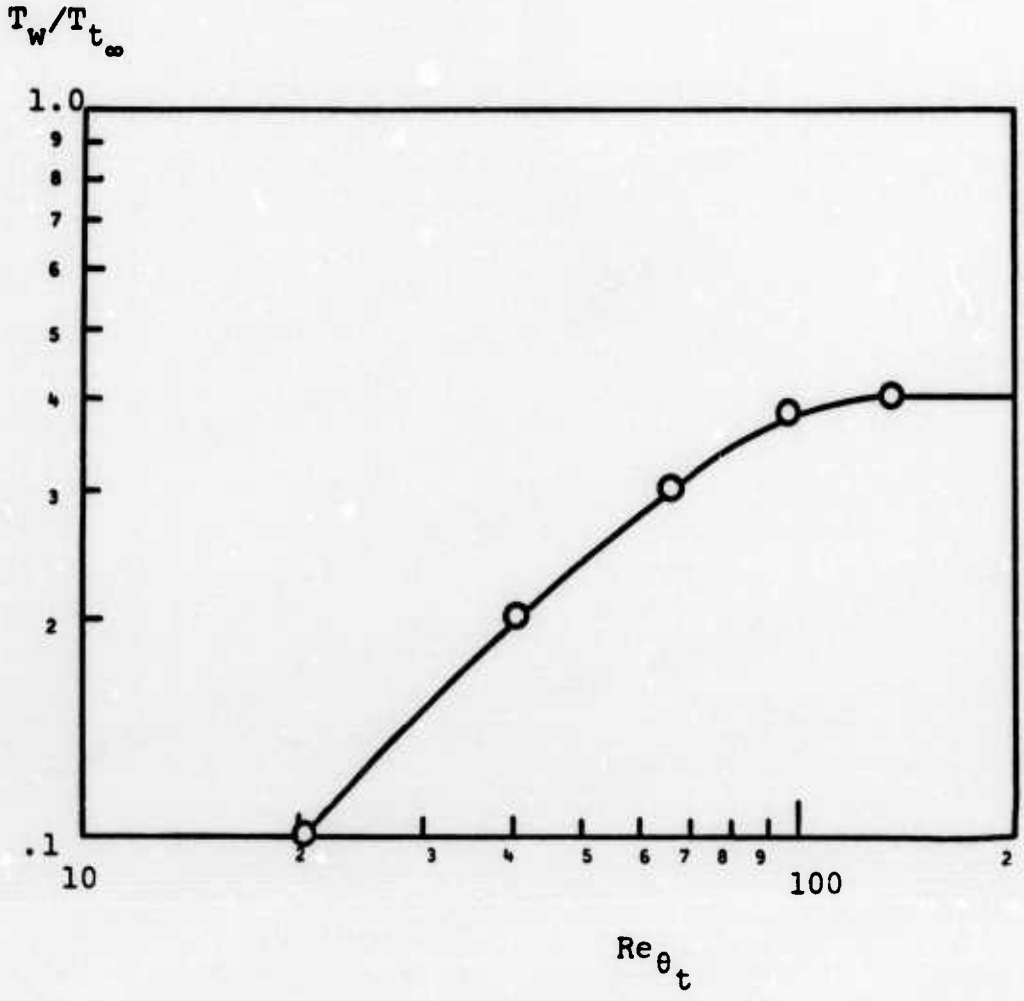

Figure 11. Effect of surface temperature on transition for constant freestream unit Reynolds number, $Re_\infty = 1.62 \cdot 10^6$ per foot.

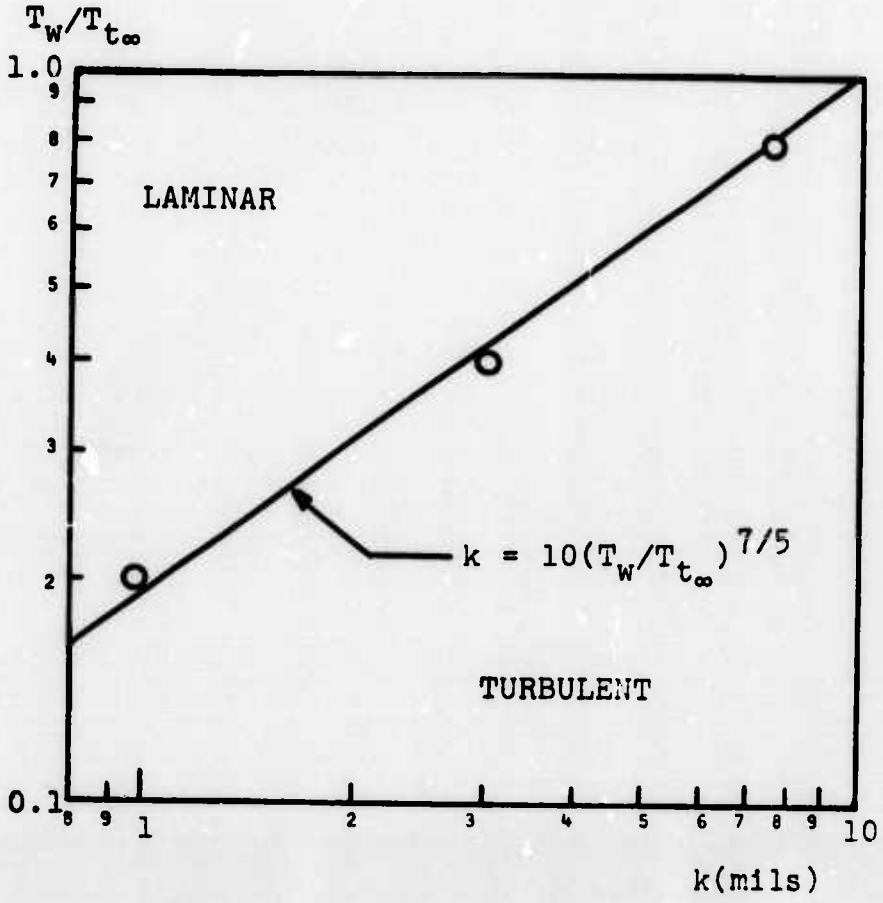

Figure 12. Minimum roughness height for incipient transition as a function of surface temperature; $Re_\infty = 1.62 \cdot 10^6$ per foot.

Table 9. Summary of nose radius calculations

r_N(in)	Re_∞(ft^{-1})	θ_{stag}(mils)	ϕ_t(°)	M_{e_t}	δ_t^*(mils)	θ_t(mils)	$\frac{k}{\theta_t}/\frac{T_w}{T_e}$	Re_{θ_t}
0.75	$2.00 \cdot 10^6$	0.74	24.75	0.55	0.42	0.80	11.05	42.4
|	$1.50 \cdot 10^6$	0.85	40.34	0.97	0.69	1.08	7.32	57.5
|	$1.48 \cdot 10^6$	0.86	43.09	1.07	0.76	1.13	6.75	60.7
|	$1.47 \cdot 10^6$	0.86	46.20	1.15	0.82	1.18	6.29	63.3
|	$1.46 \cdot 10^6$	0.86	-	-	-	-	-	∞
2.50	$1.40 \cdot 10^6$	1.61	33.56	0.78	1.07	1.87	4.47	85.6
|	$1.30 \cdot 10^6$	1.67	41.81	1.01	1.38	2.14	3.64	99.9
|	$1.28 \cdot 10^6$	1.69	47.86	1.20	1.69	2.38	3.06	110.8
|	$1.27 \cdot 10^6$	1.69	-	-	-	-	-	∞
3.50	$2.00 \cdot 10^6$	1.60	19.25	0.42	0.82	1.67	5.43	71.9
|	$1.50 \cdot 10^6$	1.85	27.70	0.62	1.09	2.04	4.29	88.2
|	$1.40 \cdot 10^6$	1.91	30.64	0.70	1.20	2.16	3.95	93.7
|	$1.35 \cdot 10^6$	1.94	33.00	0.76	1.21	2.24	3.75	98.0
|	$1.32 \cdot 10^6$	1.97	34.96	0.81	1.35	2.32	3.58	102.1
|	$1.30 \cdot 10^6$	1.98	35.75	0.83	1.39	2.35	3.50	103.3
|	$1.27 \cdot 10^6$	2.00	37.91	0.89	1.48	2.44	3.32	107.6
|	$1.23 \cdot 10^6$	2.04	42.62	1.03	1.72	2.64	2.94	116.9
|	$1.21 \cdot 10^6$	2.05	47.93	1.20	2.05	2.89	2.52	127.4
|	$1.20 \cdot 10^6$	2.06	-	-	-	-	-	∞

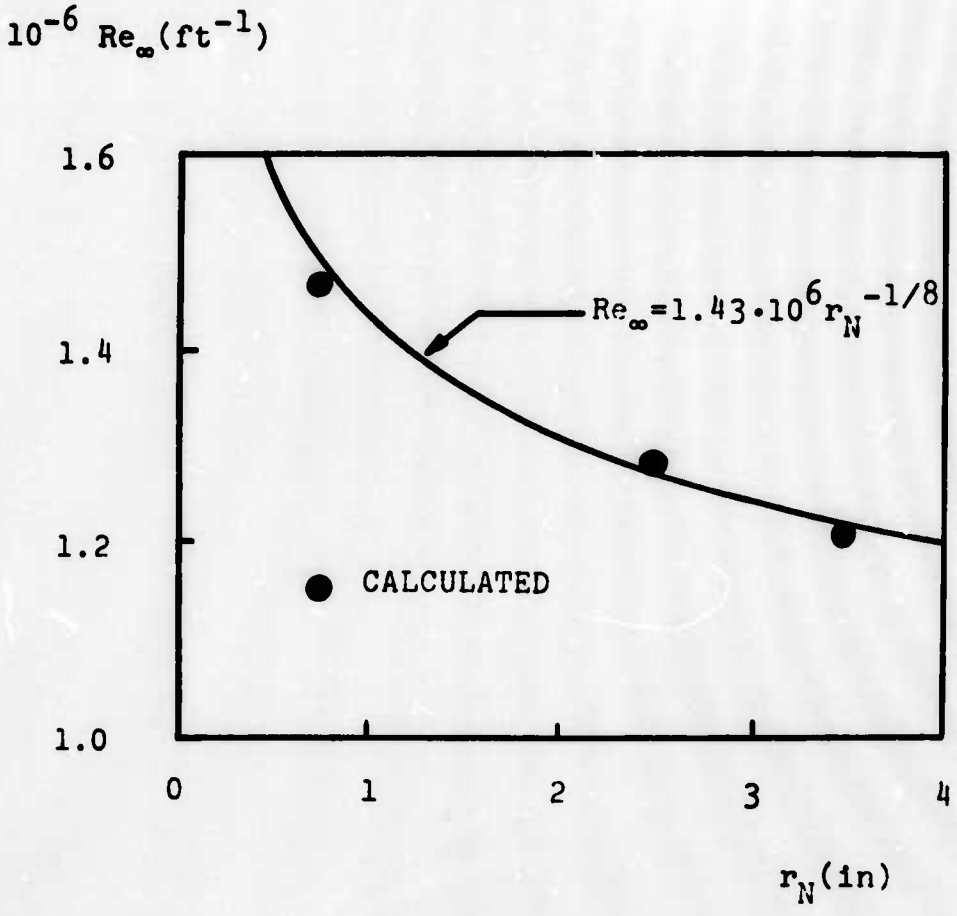

Figure 13. Dependence of incipient freestream unit Reynolds number on nose radius for sphere-cones; k=3.5 mils, T_w/T_{t_∞} = 0.373.

approximated by the following formula:

$$Re_{\infty} = 1.48 \cdot 10^{6} r_N^{-1/8} \text{ ft}^{-1} \qquad (30)$$

with r_N given in inches.

4.4 NUMERICAL NOSETIP-TRANSITION CORRELATION

All computed incipient transition points are shown in Figure 14. Six of the nine points correlate with the PANT curve [Equation (26)]. As in the PANT experiments, the 0.5-mil data point is one of the points which is not represented adequately by the curve. The other two points fail to correlate because the predicted effect of surface temperature is stronger than that indicated by the PANT curve. Figure 15 presents a new correlation which works well for all but the 0.5-mil numerical data point. Specifically, the new correlation is

$$Re_{\theta_t} = 275 \left[\frac{T_w}{T_e}\right] \left[\frac{k}{\theta_t}\right]^{-2/3} \qquad (31)$$

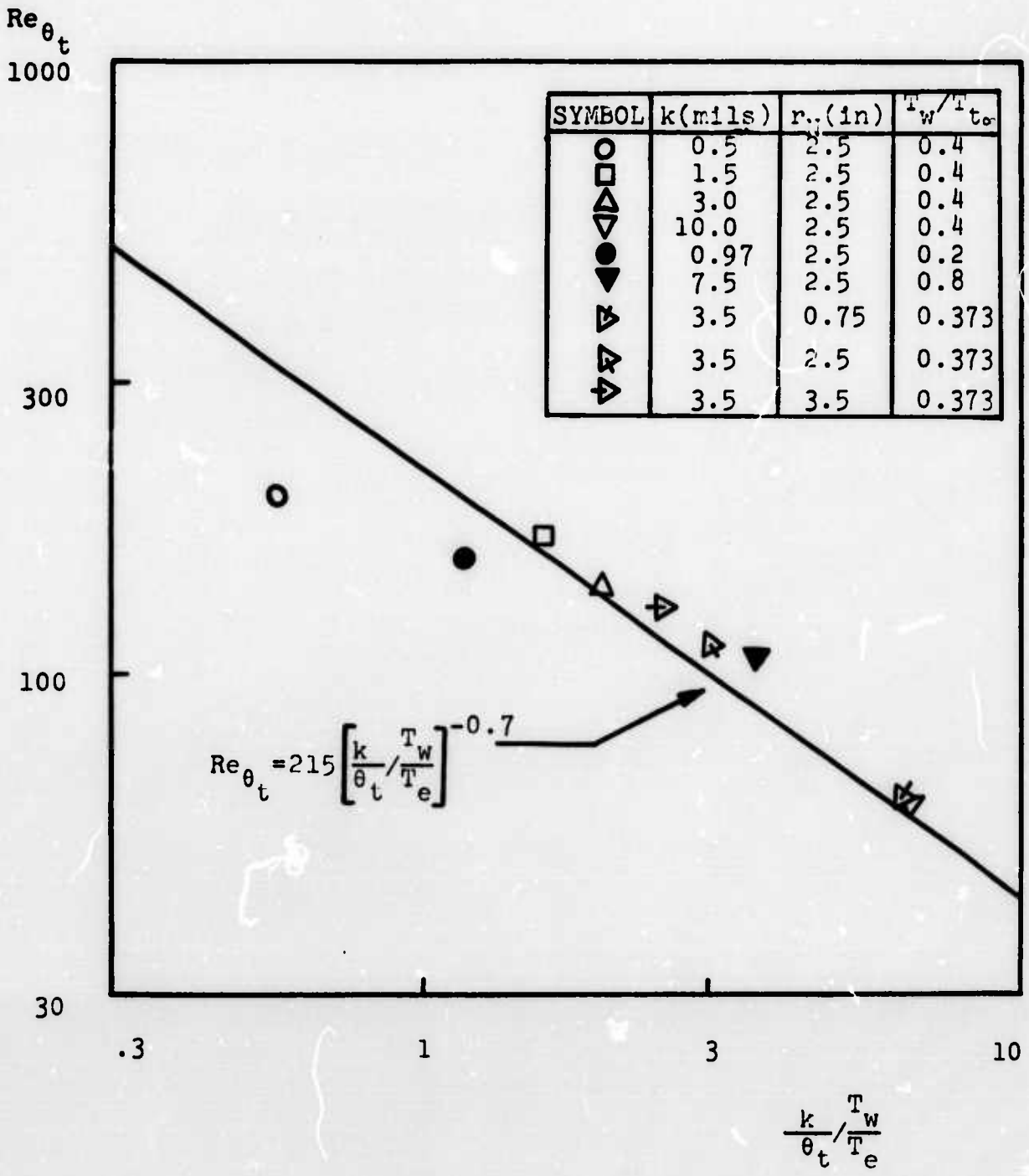

Figure 14. Comparison of computed incipient transition points with the PANT correlation.

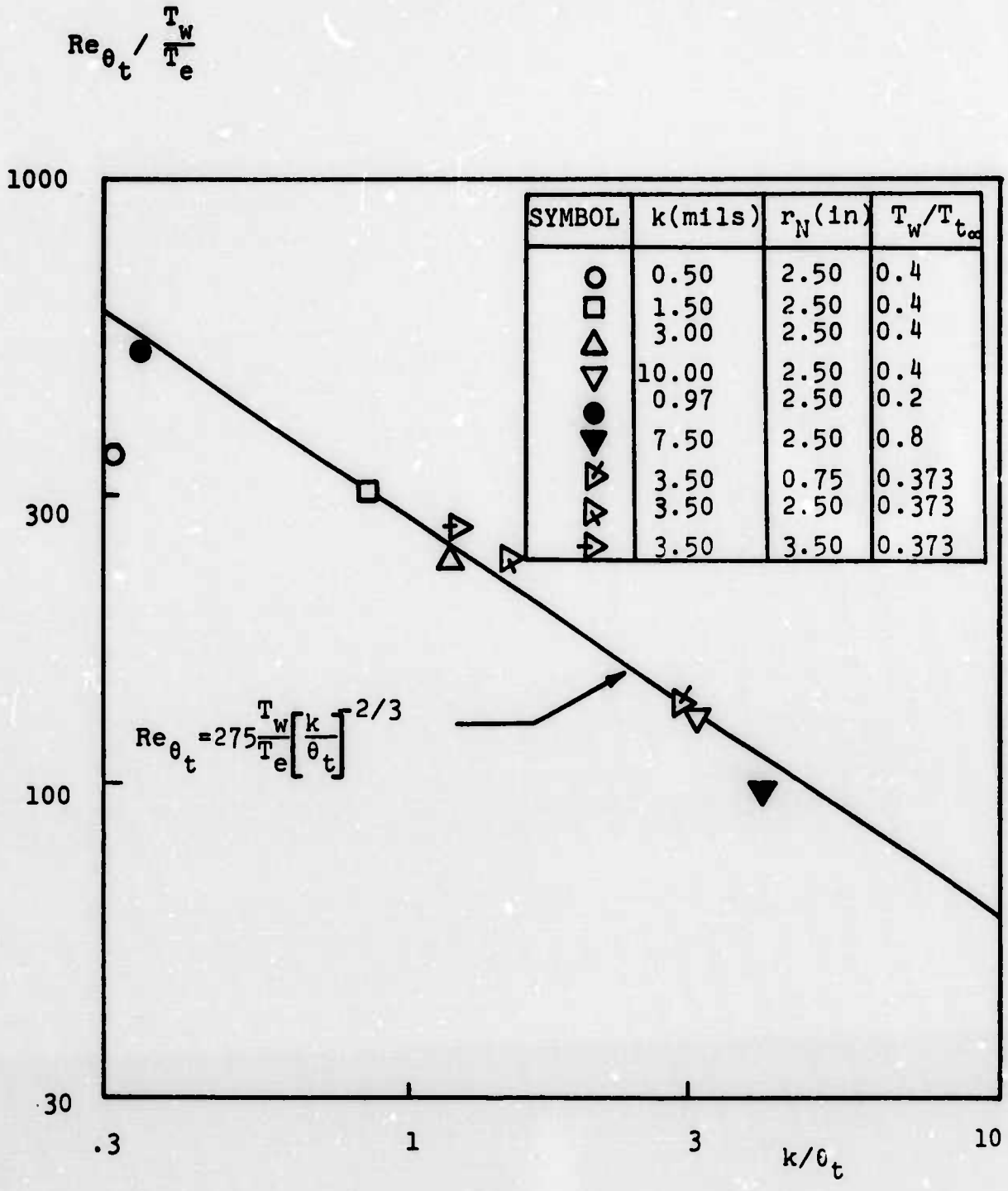

Figure 15. Incipient transition correlation inferred from numerical results for sphere-cone stagnation-region flow.

5.0 DISCUSSION

Results presented in Sections 3 and 4 show that accurate transition predictions can be made with the Saffman-turbulence-model equations, provided low-Reynolds-number effects are taken into account (Section 2). With only one adjustable parameter, namely R_o, the model yields accurate transition predictions for incompressible boundary layers and for stagnation-region flows. The effects of freestream turbulence, surface roughness, and suction on incompressible FPBL transition are well represented by the model; surface-roughness, surface-cooling, and body-geometry effects on blunt-body transition also have been predicted accurately.

The fact that the model works equally well for constant-pressure boundary layers and for stagnation-region flows is a key feature of the technique. That is, although further study will be needed to establish the model's range of applicability, the fact that the initial data base includes these <u>two</u> classes of flows provides hope that a universally applicable transition-prediction method has been developed.

Specific areas needing further model development and validation include effects on transition of freestream turbulence, compressibility and pressure gradient. As shown in Section 2, freestream-turbulence scale has a large effect on FPBL transition. While some effect is expected on physical grounds, no attempt has been made to determine whether or not the predicted effect is even qualitatively correct. Sensitivity of blunt-body transition to both freestream-turbulence intensity and scale should also be determined. The predicted role of freestream turbulence in rough-wall transition requires

further elucidation. Compressibility effects should be analyzed in detail for FPBL flows for which extensive experimental data are available. Surface cooling and freestream Mach number are easily represented with the model and should be analyzed to help test validity of the predicted stronger-than-measured effect of surface cooling on blunt-body transition. While pressure-gradient effects have been addressed indirectly by analyzing FPBL flow and the blunt-body geometric configurations, more-direct tests of the model are needed. Again, extensive experimental data exist for the effect of pressure gradient on boundary-layer transition, so that definitive tests of the model can be easily made.

In conclusion, the computations in Section 4 exemplify the turbulence-model-transition-prediction method's potential value to the reentry-vehicle-nosetip-design engineer. The EDDYBL computer code has been used in Section 4 as a "numerical wind tunnel" in that PANT Series A experiments have been simulated including a wider range of surface temperatures than could be covered in the physical tunnel. Many of the predicted results agree with measured flow properties. In particular, measured and computed effects of surface temperature on sphere-cone transition are in close agreement for the range of temperatures in the PANT experiments; however, computations at lower temperatures than those which could be considered in the PANT experiments indicate that surface cooling has a stronger effect than that inferred from the experimental data. This indicates an area in which further measurements are needed. Additionally, this exemplifies the fact that arbitrary flow conditions can be simulated in the numerical wind tunnel while the physical wind tunnel often is limited. Hence, the numerical wind tunnel can be used to test and verify the transition-prediction method for both ground-test and flight-test data and, as the ultimate goal, can be used to predict nosetip transition under real flight conditions.

APPENDIX
THE EDDYBL COMPUTER CODE

Computations in this study were performed with the EDDYBL computer code. This code is based on a boundary-layer program developed at the NASA Langley Research Center[21]; the Saffman turbulence equations were incorporated in the code in a DCW Industries research project[30]. The integration method embodied in EDDYBL is similar to the implicit Flugge-Lotz and Blottner[31] technique in which the momentum and energy equations are coupled. In adding the turbulence model to the code, the two nonlinear diffusion equations (4, 5) are solved in a coupled manner analogous to that used for the momentum and energy equations in the original version of the code. Since all four equations are not solved simultaneously, an iterative procedure is needed to obtain an accurate solution. As part of this study, a more efficient iterative procedure than had been used previously was developed.

The new iterative scheme (Figure A1) takes advantage of the special nature of transition-prediction calculations. Specifically, note that for laminar flow the momentum and energy equations are not coupled to the turbulence-density equations. Hence, with no sacrifice of accuracy, the momentum and energy equations can be solved noniteratively at each station on laminar regions. Since the turbulence density equations do require iteration when the flow is laminar, eliminating the momentum and energy equations from the iterative loop significantly reduces computing time. In specifying when all four equations must be solved iteratively, the criterion is that the maximum value (with respect to distance from the boundary) of the kinematic eddy viscosity, ε, exceed 5% of the kinematic

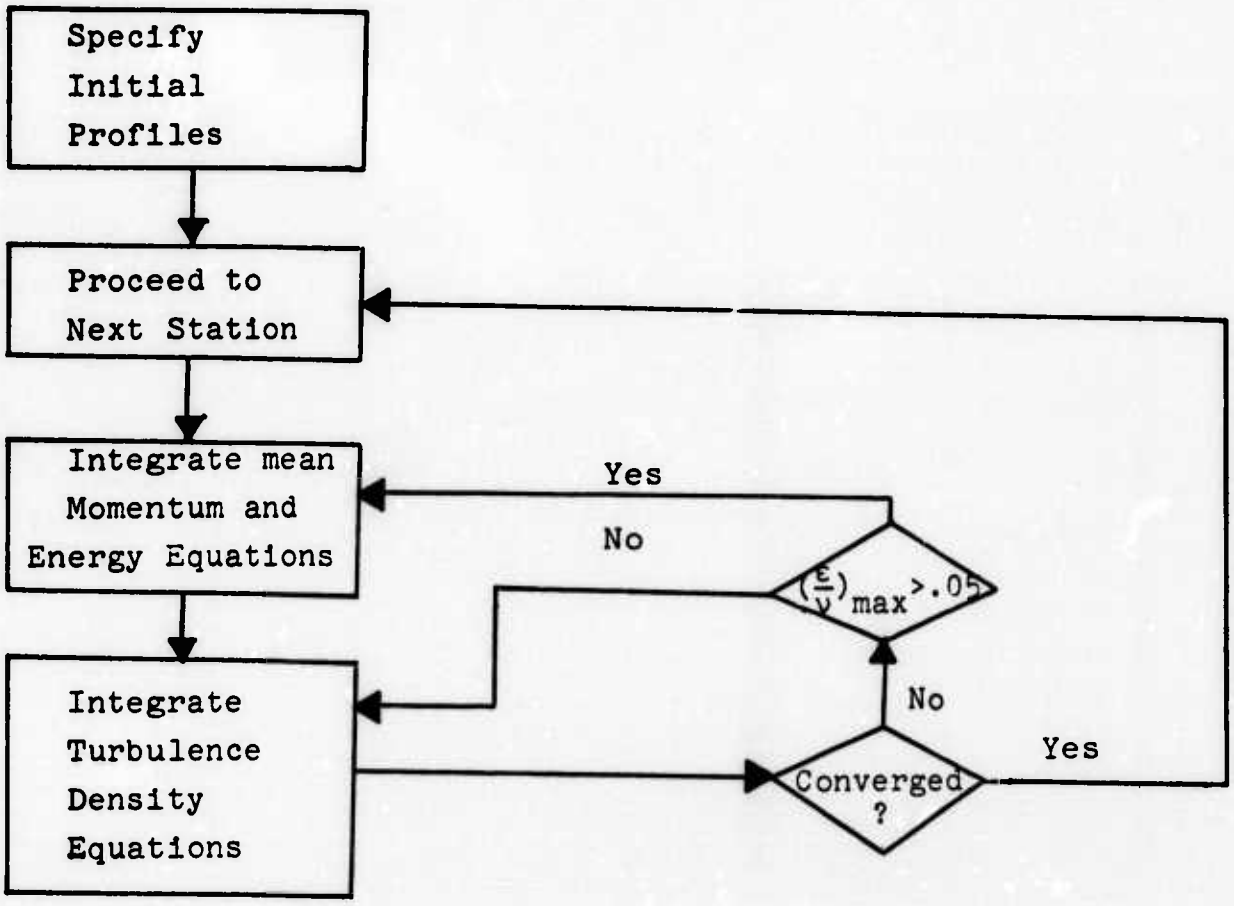

Figure A1. Schematic of iterative method used in the EDDYBL code.

molecular viscosity, ν.

Experience with EDDYBL shows that the turbulent energy converges more slowly than the other field variables. Two of the most sensitive turbulent-energy values are the peak turbulent energy and the value at the mesh point nearest the surface. These two quantities are therefore monitored to determine when convergence is attained; convergence is defined to occur when these two quantities change by less than 1% between successive iterations. Two or three iterations appear to be suitable on both laminar and turbulent regions, while seven or eight iterations typically are required through transition.

REFERENCES

1. Jackson, M.D. and Baker, D.L., "PANT Series B Wind-Tunnel Test Data Report," Aerotherm Project No. 7042, Aerotherm Acurex Corp., Mountain View, California (1972).

2. Jackson, M.D., Baker, D.L. and Powars, C.A., "PANT Series A Wind-Tunnel Test Data Report," Aerotherm Project No. 7042, Aerotherm Acurex Corp., Mountain View, California (1972).

3. Demetriades, A. and Laderman, A.J., "Final Progress Report - Advanced Penetration Problems Program," SAMSO Report No. 73-397, Space and Missile Systems Organization, Los Angeles, California (1974).

4. Laderman, A.J., "Effect of Mass Addition and Angle-of-Attack on the Hypersonic Boundary Layer Turbulence Over a Slender Come," Philco-Ford Report No. U-6047, Philco-Ford Corp., Aeronutronic Division, Newport Beach, California (1973).

5. Schubauer, G.B. and Skramstad, H.K., "Laminar Boundary Layer Oscillations and Stability of Laminar Flow," Journal of Aero. Sci. 14, p. 69 (1947).

6. Liepmann, H.W. and Fila, G.H., "Investigations of Effect of Surface Temperature and Single Roughness Elements on Boundary Layer Transition,"NACA 890 (1947).

7. Feindt, E.G., "Untersuchungen über die Abhängigkeit des Umschlages laminar-turbulent von der Oberflächenrauhigkeit und der Druckverteilung," Thesis Braunschweig 1956; Jahrbuch 1956 der Schiffbautech nischen Gesellschaft 50, pp 180-203 (1957).

8. van Driest, E.R. and Blumer, C.B., "Boundary Layer Transition: Free-Stream Turbulence and Pressure Gradient Effects," AIAA Journal, Vol. 1, pp 1303-1306 (1963).

9. Personal communication with S. Orszag, Flow Research, Inc., July 1974.

10. Schlichting, H., Boundary Layer Theory, Fourth Edition, McGraw Hill, New York (1962).

11. Mack, L.M., "On the Application of Linear Stability Theory to the Problem of Supersonic Boundary-Layer Transition," AIAA Paper 74-134 (1974).

12. Smith, A.M.O. and Gamberoni, N., "Transition, Pressure Gradient, and Stability Theory," Report ES 26388, Douglas Aircraft Co., Inc., El Segundo, California (1956).

13. Kaplan, R.E., "Generation of Turbulence-Transition," Unpublished notes, University of Southern California (1974).

14. Donaldson, C.duP., "A Computer Study of an Analytical Model of Boundary Layer Transition," AIAA Paper 68-38 (1968).

15. Jones, W.P. and Launder, B.E., "Calculation of Low Reynolds Number Phenomena with a Two-Equation Model of Turbulence," Int. J. Heat and Mass Trans. 16, pp 1119-1129 (1973).

16. Wilcox, D.C., "Turbulence Model Calculation of Rayleigh Shear Flow," DCW Industries Report DCW-R-NC-01, DCW Industries, Sherman Oaks, California (1974).

17. Saffman, P.G., "A Model for Inhomogeneous Turbulent Flow," Proc. Roy. Soc. Lond. A317, pp 417-433 (1970).

18. Wilcox, D.C. and Alber, I.E., "A Turbulence Model for High Speed Flows," Proceedings of the 1972 Heat Transfer and Fluid Mechanics Institute, Stanford Univ. Press, pp 231-252 (1972).

19. Saffman, P.G. and Wilcox, D.C., "Turbulence-Model Predictions for Turbulent Boundary Layers," AIAA Journal, Vol. 12, No. 4, pp 541-546 (1974).

20. Favre, A.J., "The Equations of Compressible Turbulent Gases," Annual Summary Report No. 1, Institute de Mechanique Statistique de la Turbulence (1965).

21. Harris, J.E., "Numerical Solution of the Equations for Compressible Laminar, Transitional, and Turbulent Boundary Layers and Comparisons with Experimental Data," NASA TR R-368 (1971).

22. Rotta, J.C., "Statistiche Theorie Nichthomogener Turbulenz," Zeitschrift für Physik, Vol. 131, pp 51-77 (1951).

23. Dryden, H.L., Aerodynamics and Jet Propulsion, V, University Press, Princeton, N.J. (1959).

24. Hall, A.A. and Hislop, G.S., "Experiments on the Transition of the Laminar Boundary Layer on a Flat Plate," ARC R&M 1843 (1938).

25. Bailey-Wright data as tabulated by Dryden in Reference 23.

26. Spangler, J.G. and Wells, C.S.,Jr., "Laminar-Boundary-Layer Oscillation and Transition on a Flat Plate," NACA 909 (1948).

27. Simpson, R.L., Moffat, R.J. and Kays, W.M., "The Turbulent Boundary Layer on a Porous Plate: An Experimental study of the Fluid Dynamics with Suction and Injection," Univ. Stanford Thermosciences Div. Report HMT-2, Stanford University (1972).

28. Pfenninger, W. and Bacon, J.W., "Investigation of Methods for Re-Establishment of a Laminar Boundary Layer from Turbulent Flow," Northrop Report NOR 65-48, Northrop Corp., Hawthorne, Calif. (1965).

29. Schlichting, H., Boundary Layer Theory, Fourth Edition, McGraw-Hill, New York, p 426 (1960).

30. Wilcox, D.C., "Turbulence-Model Transition Predictions for Compressible and Incompressible Flat-Plate Boundary Layers with Suction," DCW Industries Technical Note DCW-TN-01-01 (1974).

31. Flugge-Lotz, I. and Blottner, F.G., "Computation of the Compressible Laminar Boundary-Layer Flow Including Displacement-Thickness Interaction Using Finite-Difference Methods," AFOSR 2206 (1962).